

# P-Type Processes and Predictability

## The Winter Precipitation Type Research Multiscale Experiment (WINTRE-MIX)

Justin R. Minder<sup>✉</sup>, Nick Bassill, Frédéric Fabry, Jeffrey R. French, Katja Friedrich, Ismail Gultepe, John Gyakum, David E. Kingsmill, Karen Kosiba, Mathieu Lachapelle, Daniel Michelson, Leonid Nichman, Cuong Nguyen, Julie M. Thériault, Andrew C. Winters, Mengistu Wolde, and Joshua Wurman

**KEYWORDS:**

Mesoscale processes; Winter/cool season; Cloud microphysics; Freezing precipitation; Aircraft observations; Radars/Radar observations

**ABSTRACT:** During near-0°C surface conditions, diverse precipitation types (p-types) are possible, including rain, drizzle, freezing rain, freezing drizzle, ice pellets, wet snow, snow, and snow pellets. Near-0°C precipitation affects wide swaths of the United States and Canada, impacting aviation, road transportation, power generation and distribution, winter recreation, ecology, and hydrology. Fundamental challenges remain in observing, diagnosing, simulating, and forecasting near-0°C p-types, particularly during transitions and within complex terrain. Motivated by these challenges, the field phase of the Winter Precipitation Type Research Multiscale Experiment (WINTRE-MIX) was conducted from 1 February to 15 March 2022 to better understand how multiscale processes influence the variability and predictability of p-type and amount under near-0°C surface conditions. WINTRE-MIX took place near the U.S.–Canadian border, in northern New York and southern Quebec, a region with plentiful near-0°C precipitation influenced by terrain. During WINTRE-MIX, existing advanced mesonets in New York and Quebec were complemented by deployment of 1) surface instruments, 2) the National Research Council Convair-580 research aircraft with W- and X-band Doppler radars and in situ cloud and aerosol instrumentation, 3) two X-band dual-polarization Doppler radars and a C-band dual-polarization Doppler radar from the University of Illinois, and 4) teams collecting manual hydrometeor observations and radiosonde measurements. Eleven intensive observing periods (IOPs) were coordinated. Analysis of these WINTRE-MIX IOPs is illuminating how synoptic dynamics, mesoscale dynamics, and microscale processes combine to determine p-type and its predictability under near-0°C conditions. WINTRE-MIX research will contribute to improving nowcasts and forecasts of near-0°C precipitation through evaluation and refinement of observational diagnostics and numerical forecast models.

<https://doi.org/10.1175/BAMS-D-22-0095.1>

Corresponding author: Justin Minder, [jminder@albany.edu](mailto:jminder@albany.edu)

In final form 16 June 2023

© 2023 American Meteorological Society. This published article is licensed under the terms of the default AMS reuse license. For information regarding reuse of this content and general copyright information, consult the AMS Copyright Policy ([www.ametsoc.org/PUBSReuseLicenses](http://www.ametsoc.org/PUBSReuseLicenses)).

**AFFILIATIONS:** Minder and Bassill—University at Albany, State University of New York, Albany, New York; Fabry and Gyakum—McGill University, Montreal, Quebec, Canada; French—University of Wyoming, Laramie, Wyoming; Friedrich, Kingsmill, and Winters—University of Colorado Boulder, Boulder, Colorado; Gultepe—Environment and Climate Change Canada, Toronto, Ontario, Ontario Technical University, Oshawa, Ontario, Canada; Kosiba and Wurman—University of Illinois Urbana-Champaign, Urbana, Illinois; Lachapelle and Thériault—University of Quebec at Montreal, Montreal, Quebec, Canada; Michelson—Environment and Climate Change Canada, Toronto, Ontario, Canada; Nichman, Nguyen, and Wolde—National Research Council Canada, Ottawa, Ontario, Canada

Many people sigh, wince, or groan when they hear a forecast for a “wintry mix.” It may conjure up images of wet, slushy, and/or icy conditions that are unpleasant at best, and dangerous at worst. This nontechnical phrase implies near-0°C surface air temperatures where a diversity of precipitation types (p-types) may occur in isolation or in mixtures, including rain/drizzle, freezing rain/drizzle, ice pellets (sleet), snow, wet snow, and snow pellets (graupel). Freezing rain can be particularly impactful, as the accretion of ice onto exposed surfaces can damage utility lines and trees and degrade the safety of air and road travel (e.g., Changnon 2003; DeGaetano 2000; FAA 2015; Tobin et al. 2021). Near-0°C precipitation affects wide swaths of the United States and Canada (Cortinas et al. 2004; McCray et al. 2019; Mekis et al. 2020) and is shaped by diverse synoptic and mesoscale conditions (e.g., Bernstein 2000; Gyakum and Roebber 2001; Rauber et al. 2001; Roebber and Gyakum 2003; Henson et al. 2011; Ressler et al. 2012; McCray et al. 2020; Tootill and Kirshbaum 2022) and microscale processes (e.g., Mitra et al. 1990; Cober et al. 1996; Rasmussen et al. 2002; Milbrandt et al. 2014; Stewart et al. 2015; Reeves et al. 2016; Cholette et al. 2019).

Forecasters may have good reason to dread near-0°C precipitation events too, since forecasting p-type under such conditions can be very challenging. For instance, the summary of a U.S. Weather Research Program workshop stated that “the most serious problem with wintertime quantitative precipitation forecasting is the accurate determination of precipitation type when the surface temperature is near freezing” (Ralph et al. 2005). When temperatures are close to 0°C near the surface (or in a warm layer aloft), the surface p-type can be strongly sensitive to variations in temperature as small as  $\pm 0.5^\circ\text{C}$ , leading to fundamental predictability challenges (e.g., Thériault et al. 2010; Ikeda et al. 2013; Durran et al. 2013; Reeves et al. 2014). Even nowcasting near-0°C p-types can be challenging, as observational networks face difficulties in accurately characterizing snow, freezing drizzle, ice pellets, and mixed p-types (e.g., Rasmussen et al. 2012; Reeves et al. 2016; Landolt et al. 2019; Shin et al. 2022). These operational forecasting challenges are often exacerbated in regions of complex terrain, where orographically modified flows affect the mesoscale distribution of temperature and p-types (e.g., Roebber and Gyakum 2003; Minder and Kingsmill 2013; Thériault et al. 2015) and a lack of surface stations and near-surface radar coverage can hamper analysis efforts.

The significant impacts and challenges of near-0°C precipitation motivate some researchers to seek out “wintry mix” events for scientific study. From 1 February to 15 March 2022, a team of U.S. and Canadian scientists conducted the Winter Precipitation Type Research Multiscale Experiment (WINTRE-MIX) near Montreal, Canada. The overarching

goal of WINTRE-MIX is to better understand how multiscale processes influence the variability and predictability of precipitation type and amount under near-0°C surface conditions. In particular, WINTRE-MIX is addressing the following fundamental science questions:

- 1) How do mesoscale dynamics (especially terrain-modified flows) modulate near-0°C precipitation?
- 2) How do microscale processes modulate near-0°C precipitation?
- 3) How do multiscale processes combine to determine the predictability of near-0°C precipitation?

WINTRE-MIX efforts are also contributing to broader societal impacts through

- 1) a strengthened scientific foundation for advances in nowcasting and forecasting techniques for near-0°C precipitation events;
- 2) improved partnership between researchers, forecasters, and stakeholders; and
- 3) education and engagement of students and the general public through participation in research and outreach activities.

### Study region

WINTRE-MIX is focused on a region centered around Montreal (Fig. 1), including parts of southern Ontario and Quebec in Canada and northern New York and Vermont in the United States. This region was selected, in part, because it frequently experiences near-0°C

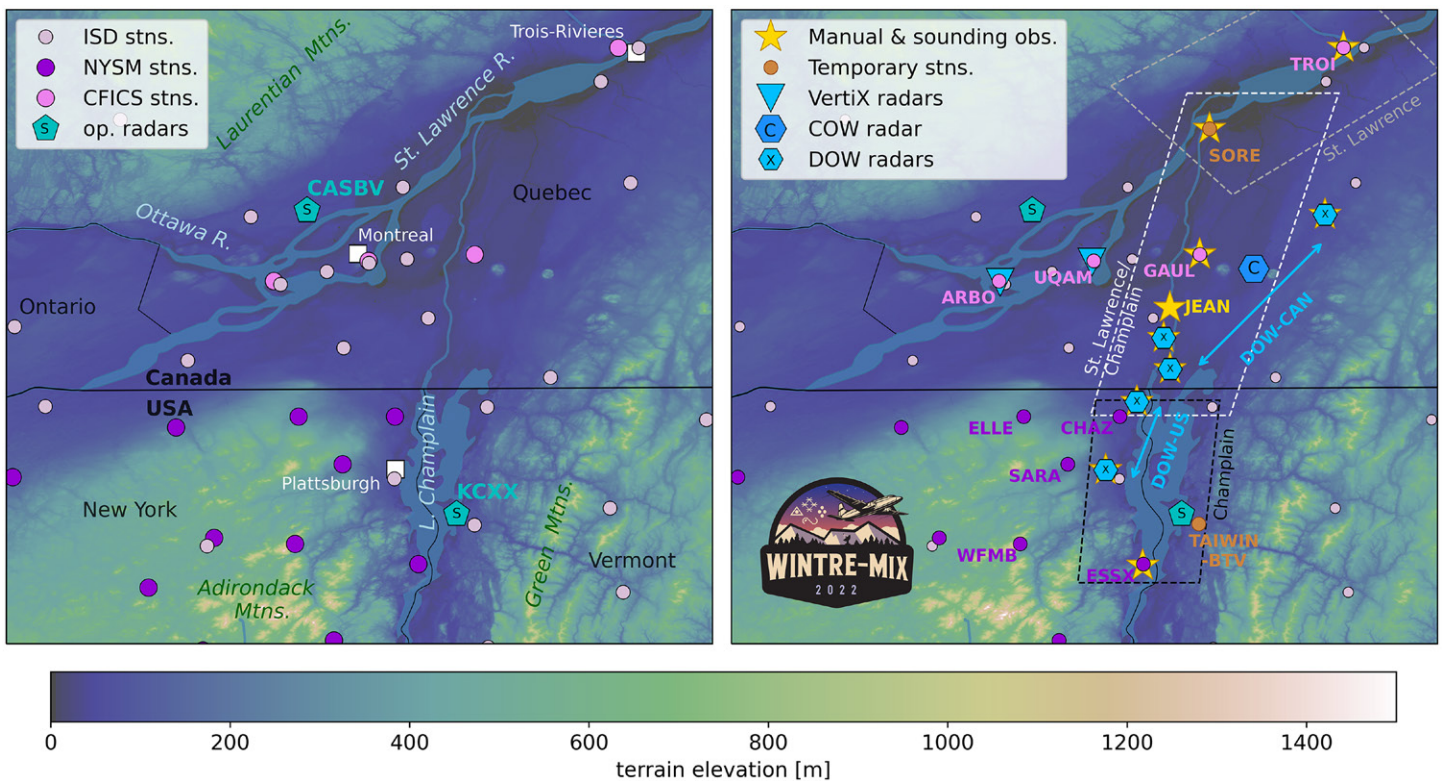


Fig. 1. Overview of WINTRE-MIX study domain with terrain. (left) Names of geographic features, operational surface stations from the Integrated Surface Database (ISD) and from local advanced mesonets (CFICS, NYSM; select stations' identifiers shown in the right panel), and S-band operational weather radars. (right) Sites of research instrumentation used for WINTRE-MIX including mobile scanning radars (X-band DOW, C-band COW), X-band profiling radars (VertiX), temporary surface station deployments, and manual and sounding observation sites. The two DOW radars shifted between multiple locations in the United States (DOW-U.S.) and Canada (DOW-CAN), respectively, as indicated by blue arrows. Dashed boxes show the approximate focus regions of operations (especially for Convair-580 flight tracks) for IOPs focused on the Champlain, Champlain–St. Lawrence, and St. Lawrence regions.

precipitation, averaging over 250 annual hours of precipitation in the  $\pm 2^{\circ}\text{C}$  temperature range, supporting a diversity of p-types (Cortinas et al. 2004; Mekis et al. 2020). For freezing rain, the region experiences more annual hours (up to 30–50 h; Fig. 2), and more events exceeding 6-h duration, than anywhere in North America except for eastern Newfoundland (McCray et al. 2019). The study domain also includes the core region impacted by the freezing rain storm of 5–9 January 1998, which led to 44 deaths, power outages affecting millions of customers, at least \$4.4 billion in economic impact, and damage to 7.1 million hectares of forest (Lott et al. 1998; DeGaetano 2000).

The WINTRE-MIX region has several topographic features that facilitate study of the influence of terrain on p-type (Fig. 1). For instance, cold-air advection by ageostrophic northeasterly flow along the St. Lawrence Valley is key for maintaining low-level sub- $0^{\circ}\text{C}$  air layers during long-duration freezing rain events (e.g., Roebber and Gyakum 2003; Ressler et al. 2012; McCray et al. 2019). Channeled flow also affects p-type in the Champlain Valley and contributes to mesoscale frontogenesis that may enhance precipitation near the confluence of the two valleys (e.g., Roebber and Gyakum 2003). Orographic ascent or descent along the slopes of the neighboring Adirondacks, Laurentians, and Green Mountains can further shape the mesoscale distribution of temperature, p-type, and precipitation intensity in the region (e.g., Henson et al. 2011).

Existing operational networks provided a strong observational foundation for WINTRE-MIX to build upon (Fig. 1). In particular, dual-polarization S-band scanning radars in the United States (KCXX) and Canada (CASBV) provide surveillance coverage for kinematic and microphysical monitoring of storms, while surface stations provide routine meteorological measurements, including multisensor p-type diagnosis, largely at airports within the valleys (e.g., NOAA 1998). The region is also home to two advanced regional mesonets: the New York State Mesonet (NYSM; Brotzge et al. 2020) and the Canada Foundation for Innovation Climate Sentinels (CFICS). Variables measured at advanced mesonet sites in the core WINTRE-MIX domain are summarized in Table 1 and example site photos are shown in Figs. 3e, 3k, and 3l. Liquid equivalent precipitation is measured for all p-types within both mesonets using either a weighing gauge with a double-Alter wind shield (NYSM sites) or a hot plate precipitation gauge (CFICS sites). Icing occurrence and icing rates are measured using an icing detector at CFICS sites. Under certain conditions, icing can be detected at NYSM sites by comparing measurements from their collocated sonic and propeller anemometers (Wang et al. 2021). Select NYSM and CFICS sites also document conditions above the surface via radar, lidar, and/or radiometer remote sensing measurements that retrieve vertical profiles of temperature, humidity, winds, and/or radar variables.

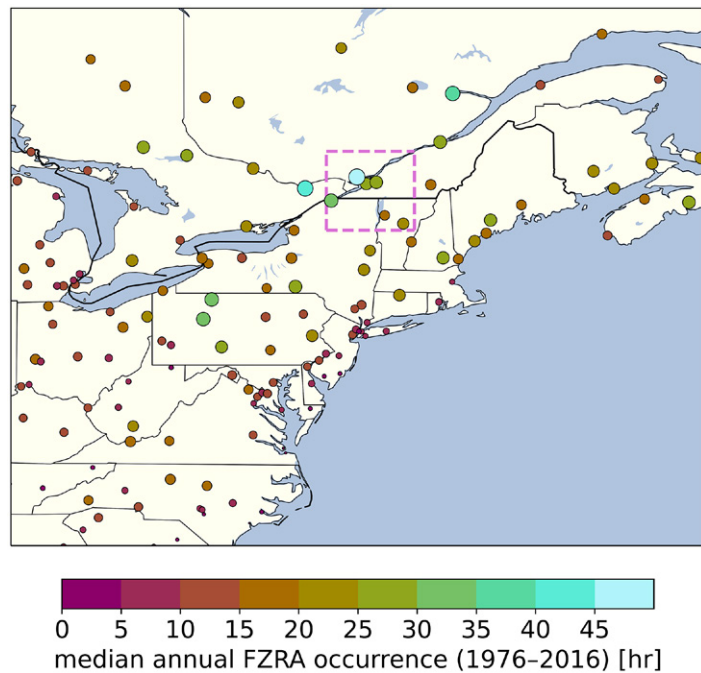


Fig. 2. Median annual hours of freezing rain (FZRA) in the northeastern United States and southeastern Canada, adapted from McCray et al. (2019). Dashed box shows the approximate domain of focus for WINTRE-MIX.

**Table 1. Summary of instrumentation at primary surface observation stations used during WINTRE-MIX. Temp. = temperature; hum. = humidity. An asterisk indicates stations or sensors deployed specifically for WINTRE-MIX. Locations of stations are indicated in Fig. 1.**

	NYSM stations (CHAZ, SARA, ELLE, ESSX, WFMB)	CFICS stations (GAUL, UQAM, ARBO, TROI <sup>a</sup> )	Sorel* (SORE)
Temperature, humidity	Temp. and hum. at 2 m, temp. at 9 m	Temp. and hum. at various heights (GAUL) <sup>b</sup> , temp. at various heights (ARBO) <sup>c</sup> , temp. and hum. at 2.2 m (UQAM) <sup>d</sup> , temp. and hum. at 2.0 m (TROI)	Temp. and hum. at 2 m
Winds	Sonic and prop-vane at 10 m	Sonic at 10 m (GAUL, ARBO), prop-vane at 10 m (GAUL, ARBO, UQAM)	Sonic at 2 m
Radiative fluxes	Shortwave down (all), shortwave and longwave up and down (CHAZ)	Shortwave down (all), net (GAUL, ARBO, UQAM), shortwave and longwave up and down (TROI, UQAM)	
Turbulent fluxes	Sensible and latent (CHAZ)	Sensible and latent (GAUL, ARBO)	
Total precipitation	Weighing gauge with double-Alter shield	Weighing gauge (UQAM), hot plate (GAUL, ARBO, UQAM, TROI)	Weighing gauge w/single-Alter shield
Snowpack	Depth–sonic sensor (all), water equivalent–gamma sensor (WFMB)	Depth–sonic sensor (GAUL, TROI), water equivalent–gamma sensor (GAUL), SDMS40 (GAUL, UQAM, ARBO)	
Ice accretion	Rosemont 0871LH1*	Goodrich 0872F1	
Precipitation disdrometer	Parsivel <sup>2</sup> (CHAZ)*	Parsivel <sup>2</sup>	Parsivel <sup>1</sup>
Visibility		CS120A (GAUL, ARBO, UQAM)	Vaisala FD70p
Radar profiles	MRR-2 (CHAZ)*	MRR-2 (GAUL, ARBO, UQAM), MRR-Pro (TROI)	MRR-Pro
Lidar profiles	Leosphere Windcube Doppler lidar (CHAZ)	CS125 ceilometer (GAUL, ARBO)	Halo Streamline Doppler lidar
Radiometer profiles	Radiometrics MP-3000 (CHAZ)		Radiometrics MP-3000

<sup>a</sup> TROI used equipment from a UQAM urban mobile station specifically deployed for WINTRE-MIX, which served as a precursor to a permanent CFICS station at the same site.

<sup>b</sup> Measurement heights: 1, 1.5, 2, 3.5, 4.5, 5, 8, 10 m.

<sup>c</sup> Measurement heights: 0.2, 0.6, 1.1, 1.75, 3.6, 5.5, 10 m.

<sup>d</sup> Height is relative to rooftop platform.

## Instruments deployed

WINTRE-MIX supplemented the above-described operational network to provide a denser and specialized observational network to monitor conditions at the surface and aloft. The core facilities deployed were an instrumented research aircraft and three mobile radars. These core facilities were complemented by a range of manual and automated ground-based measurements. During the primary observation period, 1 February–15 March 2022, 11 intensive observing periods (IOPs) were conducted. IOPs are defined as any period when scientific data were collected from the mobile radars, the aircraft, or sounding teams during a near-0°C precipitation event.

**Research aircraft: NRC Convair-580.** During WINTRE-MIX, airborne observations were used to characterize mesoscale variations in winds and atmospheric state as well as aerosol, cloud, and precipitation properties. The National Research Council Canada (NRC) Convair-580 research aircraft (Fig. 3a; Nguyen et al. 2022) flew nine missions (approximately 40 research flight hours) in support of WINTRE-MIX. The Convair-580 carried an extensive suite of in situ and remote sensing instruments (Table 2). The NRC team has substantial experience collecting data in challenging mixed-phase cloud and precipitation environments targeted by WINTRE-MIX, including during the recent In-Cloud Icing and Large Drop Experiment (ICICLE; Bernstein et al. 2021).

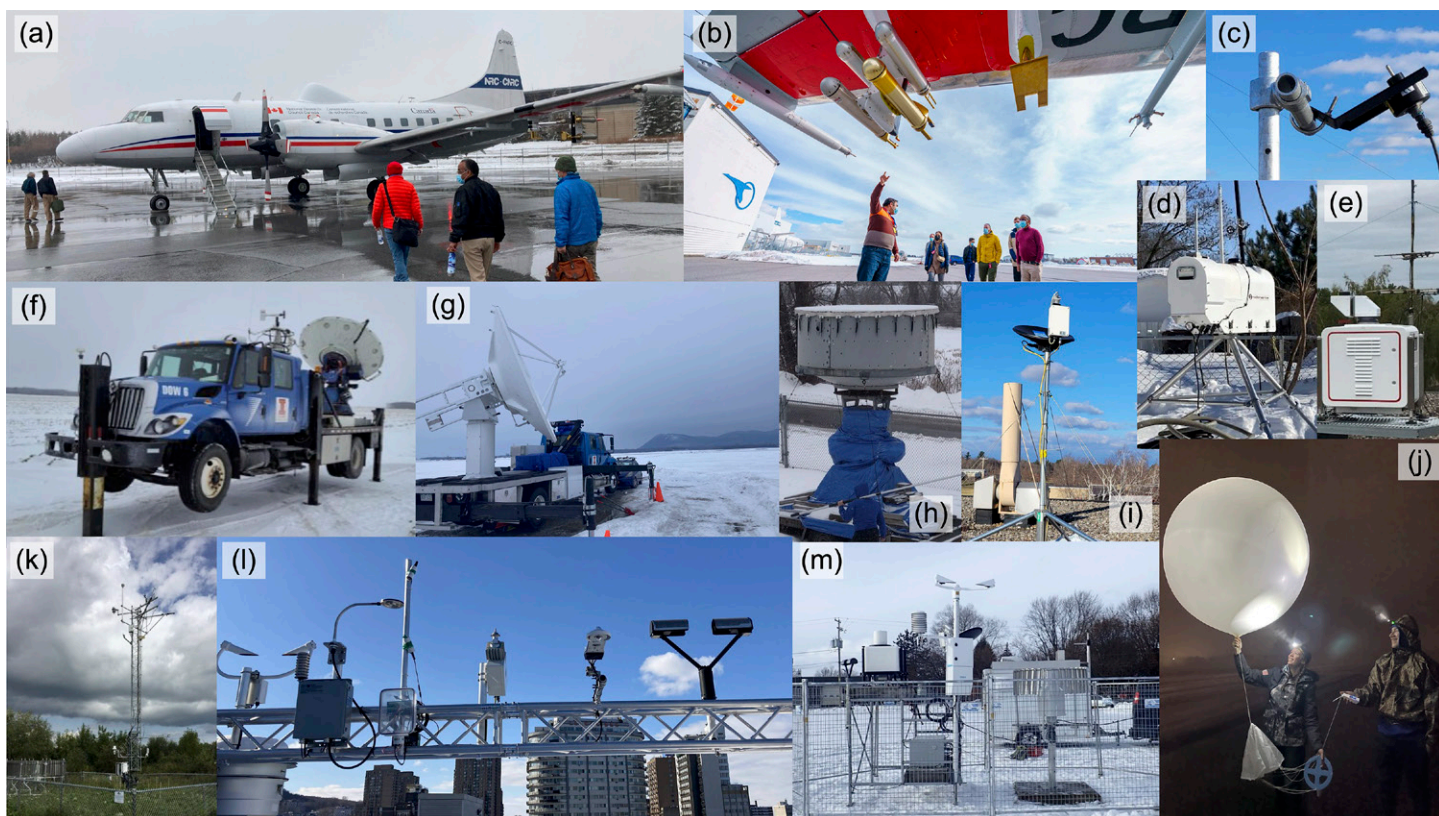


**Fig. 3.** Examples of core instrumentation used during WINTRE-MIX. (a) Convair-580 research aircraft; (b) wing-mounted probes on the Convair-580 for in situ measurements; (c) Rosemont icing detector at Chazy, NY, NYSM station (CHAZ); (d) microwave radiometer at Sorel, QC (SORE); (e) Doppler lidar at CHAZ; (f) DOW-U.S. mobile radar; (g) COW mobile radar; (h) VertiX profiling radar; (i) MRR-2 profiling radar at CHAZ; (j) UAlbany undergraduate students launching a radiosonde at Plattsburgh, NY; (k) NYSM station at CHAZ; (l) some of the sensors comprising the CFICS station at Montreal, QC (UQAM); (m) temporary station deployed at SORE. Locations of stations and radars are shown on Fig. 1.

In situ probes provided measurements along the aircraft flight track of bulk liquid and ice water content, imagery and size distributions of hydrometeors, 3D wind and turbulence, and atmospheric state. Cloud and precipitation particle concentration, phase discrimination, and habit identification were provided by a combination of scattering and optical array probes (e.g., Fig. 3b). Bulk measurements of liquid and ice content were provided by hotwire probes, including a deep-cone Nevzorov (Korolev et al. 2013). Aerosol size distributions from outside of cloud were provided by a wing-mounted Ultra-High Sensitivity Aerosol Spectrometer (UHSAS; Cai et al. 2008). In-cloud residual aerosol data were collected behind a Counterflow Virtual Impactor (CVI) inlet system (Shingler et al. 2012). These measurements included aerosol particle size distribution, cloud condensation nuclei activity, composition, and total concentration.

The aircraft has three integrated remote sensing instruments: a W-band cloud radar (NAW), an X-band precipitation radar (NAX), and an elastic backscatter cloud lidar (Wolde and Pazmany 2005; Wolde et al. 2019; Baibakov et al. 2016). The NAW has a nominal resolution of 30–50 m and a minimum detectable signal of  $-30$  dBZ at 1-km range. The radar can operate using three antennas simultaneously: down, side, and either up- or forward-of-down-pointing. During WINTRE-MIX, two configurations were primarily used: 1) up, down, side and 2) down, down-forward, side. The first configuration was used to retrieve full vertical profiles of the cloud and the second configuration was used to retrieve horizontal and vertical hydrometeor motion in the 2D plane along and below the flight track (e.g., following Damiani and Haimov 2006). The NAX has a similar profiling capability, but is only sensitive to precipitation, providing information on the vertical profile of hydrometeors and their phase. The cloud lidar

**Table 2. Summary of instrumentation flown on the NRC Convair-580 during WINTRE-MIX.**

Category	Instrument	Parameters	Notes
In situ cloud and precipitation properties	Nevzorov	Liquid and total water content	Bulk cloud properties
	ICD (WCM-4000)	Liquid and total water content	Bulk cloud properties
	Rosemount Icing Detector (×2)	Icing indicator	
	Cloud Droplet Probe (CDP-2)	Size range: 3–50 μm	Forward scattering
	Fast CDP (FCDP)	Size range: 1.5–50 μm	Forward scattering
	2D-S (Stereo) Probe	Size range: 10–1,280 μm	Cloud particle imaging
	Cloud Imaging Probe (CIP-15)	Size range: 25–1,550 μm	Cloud particle imaging
	Precipitation Imaging Probe (PIP)	Size range: 100–6,400 μm	Precipitation particle imaging
Aerosol	High Volume Precipitation Spectrometer (HVPS-3)	Size range: 150–19,200 μm	Precipitation particle imaging
	Ultra-High Sensitivity Aerosols Spectrometer (UHSAS) (×2)	Aerosol size distribution (0.06 nm–1 μm)	One wing mounted, one cabin mounted
	Counter-flow Virtual Impactor (CVI) inlet system	Hydrometeors > 8 μm	Enables sampling of residual aerosol
	Condensation Particle Counter (CPC)	Total aerosol concentration	Cabin mounted
	Single Particle Soot Photometer (SP2)	Aerosol composition	Cabin mounted
	Cloud Condensation Nuclei Counter (CCNc)	CCN concentration, hygroscopicity	Cabin mounted, constant pressure inlet
Atmospheric state	RMNT Pressure Transducer (×2)	Static and dynamic pressure	One fuselage mounted, one wing boom mounted
	RMNT TAT (×3)	Temperature	Two wing boom mounted, one under wing boom
	AIMMS-20 Air Data Probe (ADP)	Temperature, pressure, RH, airflow incidence angles	Wing tip mounted
	RMNT 858 ADP, Aeroprobe ADP	Pressure, airflow incidence angle	Mounted on wing boom
	LICOR 840a, LICOR 7000	Water vapor concentration, dewpoint	Cabin mounted
	Vigilant Chilled-Mirror Hygrometer	Dew/frost point	Cabin mounted
Aircraft state	GPS (×2)	Position	
	Inertial Measurement Unit (IMU) (×3)	Aircraft inertial state	
Remote sensing	NAW W-band radar (94.05 GHz)	Equivalent reflectivity factor, Doppler velocity	Pointing directions: up, down, side
	NAX X-band radar (9.41 GHz)	Equivalent reflectivity factor, Doppler velocity	Pointing directions: up, down, side
	Airborne Elastic Cloud lidar (AECL) (355 nm)	Lidar backscatter and depolarization ratio	Pointing direction: up

provided vertical profiles, above the aircraft, of co-polarized and cross-polarized attenuated backscatter that can be used to identify layers of cloud liquid water away from the aircraft flight level.

Aircraft sampling was primarily conducted along predefined straight flight legs at constant altitudes, focused on either the St. Lawrence Valley, the Champlain Valley, or the confluence between the two (e.g., Fig. 1). Flight legs were typically oriented relative to the terrain, along valley or cross valley. These terrain-relative leg orientations were used to facilitate sampling of orographic effects on kinematic, thermodynamic, and microphysical storm characteristics. The legs were designed to pass over ground-based WINTRE-MIX assets, including profiling and scanning radars, to facilitate synergistic measurements. Along-valley legs were often flown at multiple altitudes, sampling temperature levels from +3° to –15°C, to document vertical variations in microphysical properties, including within

melting layers. Additionally, missed approaches were used at airports in the St. Lawrence and Champlain Valleys to obtain vertical profiles of near-surface conditions, including elevated warm layers, where melting occurred, and near-surface cold layers, where liquid water became supercooled or refroze.

**Mobile radars: FARM DOWs/COW.** Mobile radars were used to provide continuous high-resolution measurements of the mesoscale structure and organization of precipitation systems and their kinematic and microphysical characteristics. Three radars from the University of Illinois Urbana–Champaign Flexible Array of Radars and Mesonets (FARM; Wurman et al. 2021) were deployed. These included two dual-polarization X-band Doppler On Wheels radars (DOWs, Fig. 3f) and a dual-polarization C-band Doppler radar (COW, Fig. 3g). The COW radar was deployed at a fixed location in the St. Lawrence Valley, near the center of the WINTRE-MIX study domain. In contrast, the two DOW radars were deployed to various locations depending on the forecasted weather conditions and scientific goals of each IOP, with one deployed in the St. Lawrence Valley (DOW-CAN) and one deployed in the Champlain Valley (DOW-U.S.). Deployment locations are shown in Fig. 1.

During WINTRE-MIX, radar operations and scan strategies were optimized to sample mixed precipitation weather conditions and provide observations along the flight track and over the ground-based observation sites (Table 3). Research radar volume (plan position indicator, PPI) scans ranging from 0.4° to 50° elevation angle were synchronized every 6 min with the operational Environment Climate Change Canada (ECCC) radar in Blainville, Canada. Within their 6-min scan cycle, research radars also conducted vertical cross-section (range–height indicator, RHI) scans approximately perpendicular to and along the Convair-580 flight track and a vertical scan at 89° elevation. When siting the radars, it was not possible to completely avoid low-level beam blockage from nearby terrain, vegetation, and structures. Data with ground-clutter contamination and partial/full beam blockage were removed afterward using texture and thresholds of dual-polarization variables. Multiple radar PPI scans are being used to conduct multiradar synthesis (e.g., dual-Doppler analyses), to map three-dimensional variations in precipitating systems, and derive the vertical profile of horizontal winds at the radar location (via velocity–azimuth display analysis).

**Manual observation and sounding teams.** Four teams stationed throughout the WINTRE-MIX domain launched soundings and collected manual hydrometeor observations. These teams were led (and primarily staffed) by students or postdocs from University at Albany (UAlbany), University of Colorado Boulder (CU), University of Quebec at Montreal (UQAM), and McGill University (e.g., Fig. 3j). The McGill team was stationed at the Gault CFICS site for all IOPs. The UQAM team was primarily stationed at the Sorel ground observation site, though they also collected data at other sites, including Trois-Rivières, during IOPs 5, 8, and 11. The UAlbany and CU teams deployed with the DOW radars in the Champlain

**Table 3. Summary of mobile radar technical specifications and configurations used during WINTRE-MIX. Note, the COW and DOW radars each operated at two different frequencies, indicated as high and low, with corresponding Nyquist velocities.**

	COW	DOW-CAN and DOW-U.S.
Frequency	5.40 GHz (low), 5.55 GHz (high)	9.3 GHz (low), 9.5 GHz (high) <sup>a</sup>
Gate length	75 m	75 m
Max range	89 km	75 km
Nyquist velocity	69.4 m s <sup>-1</sup> (low), 67.5 m s <sup>-1</sup> (high)	40.1 m s <sup>-1</sup> (low), 39.4 m s <sup>-1</sup> (high) <sup>a</sup>
Resolution	0.5° (PPIs), 0.2° (RHIs)	0.5° (PPIs), 0.2° (RHIs)

<sup>a</sup> DOW-U.S. only.

and St. Lawrence Valleys, respectively. This distribution of observation locations (Fig. 1) facilitated sampling conditions along the major valleys and across p-type transition boundaries. Soundings characterized spatial and temporal variations in the vertical profile of thermodynamic conditions, which exert fundamentals control on p-type (e.g., Zerr 1997) as well as kinematic and thermodynamic variations associated with terrain modified flows and frontal features (e.g., Roebber and Gyakum 2003). For all IOPs, environmental soundings were conducted at one or two locations to sample the environment prior to or at the beginning of an IOP. Sites that did not conduct an initial environmental sounding typically began their sounding operations at the start of radar observations. Soundings were conducted simultaneously at all sites at intervals between 1 and 2 h.

Manual hydrometeor observations provided ground truth measurements of sensible weather conditions during WINTRE-MIX, which were vital due to the inherent difficulties in making accurate automated measurements of p-type, snow accumulation, and ice accretion. Manual hydrometeor observations were recorded every 10 min throughout the duration of IOPs. These observations included primary and secondary p-type, cloud type and cover, snow accumulation, and ice accretion. To aid in real-time visualization of the data, the teams also submitted their p-type observations via the mPING app (Elmore et al. 2014). Snow depth and liquid water equivalent were measured typically every 2 or 3 h using a snowboard that was cleared between measurements. When freezing rain or freezing drizzle was present, total radial ice accretion was measured on a metal rod throughout the duration of the IOP. When frozen precipitation (snow, ice crystals, snow pellets, or ice pellets) was present, hydrometeors were collected on a black velvet pad and photographed using a digital SLR camera with a macro lens, following the procedures of Gibson and Stewart (2007) and Lachapelle and Thériault (2022).

**Other ground-based sensors.** Various other automated ground-based instruments collected data during WINTRE-MIX, complementing the measurements described above. These instruments included preexisting research deployments, augmentations to existing stations made for WINTRE-MIX, and the deployment of a temporary research station (e.g., Table 1). Two VertiX X-band profiling Doppler radars (e.g., Fig. 3h), operated by McGill University, collected data in Montreal and adjacent to the ARBO CFICS site (Fig. 1). At Sorel, Quebec, a temporary station was established by ECCC, UQAM, and CU (Figs. 3d,m). This site included instruments previously used for research on freezing fog and precipitation that provided measurements of surface meteorology, visibility, and precipitation size/velocity distributions (Gultepe et al. 2019). The Sorel site also included profiling measurements of microphysical properties, winds, and thermodynamics from a vertically pointing Micro Rain Radar (MRR)-Pro radar, a Doppler lidar, and a microwave radiometer. In northeastern New York, five NYSM sites were augmented with Rosemont icing detectors to measure icing occurrence and ice accretion (e.g., Fig. 3c). At the Chazy NYSM site, a profiling MRR-2 radar (Fig. 3i) and optical disdrometer were also deployed. In Burlington, Vermont, the FAA TAIWIN Demonstration Project augmented existing Automated Surface Observing System (ASOS) observations with optical disdrometer, profiling radar, icing, and weighing precipitation gauge measurements (for more about FAA-TAIWIN, see sidebar).

## Field operations

The timing of IOPs was determined based on the suitability of forecasted weather for answering core science questions, the availability of resources, and crew duty limitations. In planning, executing, and reviewing IOPs, the WINTRE-MIX team made extensive use of a field catalog developed by the NCAR Earth Observing Laboratory to review forecasts, real-time observations, instrument status, and summary reports (<http://catalog.eol.ucar.edu/wintre-mix>).

## Synergies with overlapping campaigns

WINTRE-MIX coordinated with two other winter weather field projects operating in overlapping regions and periods. The NASA Investigation of Microphysics and Precipitation for Atlantic Coast-Threatening Snowstorms (IMPACTS) Campaign (McMurdie et al. 2022) was studying snowband processes in winter cyclones during January–February 2022. IMPACTS conducted two airborne missions studying clipper systems wherein their research aircraft flew over WINTRE-MIX ground assets in Quebec and provided complementary data. During IOP 6, WINTRE-MIX deployed a DOW radar and manual observation team to the southern Champlain Valley to collect data in coordination with an IMPACTS mission.

The Federal Aviation Administration conducted the Terminal Area Icing Weather Information for NextGen demonstration project (TAIWIN-Demo) to test and improve a diagnostic tool being developed to mitigate aviation icing hazards (e.g., Bernstein et al. 2021). It took place from 25 January to 25 February 2022 and used the Convair-580 to conduct research flights over New York State. WINTRE-MIX worked closely with TAIWIN-Demo to share data and use of the Convair-580 facility. Data collected have already been used in simulations of in-flight ice accretion hazard, toward prevention of surface icing, and development of sensors and protection solutions (e.g., Nichman et al. 2023).

Eleven IOPs were conducted, as summarized in Table 4. Nine of the IOPs included Convair-580 research flights and one (IOP 9) included two flights. Another (IOP 6) involved operations outside of the normal WINTRE-MIX domain and collaborations with two other winter weather field campaigns: NASA-IMPACTS and FAA-TAIWIN (see sidebar). All three mobile radars operated for most IOPs. For IOPs 10 and 11, the COW radar did not operate because it needed to depart for a different field deployment.

The geographic focus varied between IOPs, with five IOPs focusing on a domain spanning the St. Lawrence and Champlain Valleys, four IOPs focusing primarily in the St. Lawrence

**Table 4. Overview of WINTRE-MIX IOPs. Time range is the span of time when airborne, sounding, or mobile radar observations were collected. Focus regions, mobile radar sites, and manual/sounding sites are indicated in Fig. 1. P-types indicates the types of precipitation observed manually at WINTRE-MIX ground observation sites [RA = rain; FZRA = freezing rain; DZ = drizzle; FZDZ = freezing drizzle; SN = snow; SG = snow grains; IC = ice crystals; PL = ice pellets; GS = snow pellets (graupel)].**

IOP	Time range	Focus region	Aircraft	Mobile radars	Manual and sounding sites	P-types
1	2100 UTC 2 Feb–900 UTC 3 Feb	St. Lawrence/Champlain	Yes	COW, DOW-CAN, DOW-U.S.	SORE, GAUL, DOW-CAN, DOW-U.S.	DZ, RA, FZRA, SN
2	0800–1330 UTC 10 Feb	St. Lawrence	No	COW, DOW-CAN, DOW-U.S.	SORE, GAUL, DOW-CAN, DOW-U.S.	DZ, PL, SG, SN
3	2200 UTC 11 Feb–0630 UTC 12 Feb	St. Lawrence	Yes	COW, DOW-CAN, DOW-U.S.	SORE, GAUL, DOW-CAN, DOW-U.S.	DZ, RA
4	2300 UTC 17 Feb–1000 UTC 18 Feb	Champlain	Yes	DOW-CAN, DOW-U.S.	SORE, GAUL, COW, DOW-CAN, DOW-U.S.	DZ, RA, FZRA, PL, SN, GS
5	2100 UTC 22 Feb–0530 UTC 23 Feb	St. Lawrence	Yes	COW, DOW-CAN, DOW-U.S.	TROI, SORE, GAUL, COW, DOW-CAN, DOW-U.S.	DZ, RA, FZDZ, FZRA, PL, IC
6	0900–1500 UTC 25 Feb	Champlain (& western NY)	Yes <sup>a</sup>	DOW-U.S. <sup>b</sup>	ESSX <sup>b</sup>	SN
7	1600 UTC 1 Mar–0200 UTC 2 Mar	St. Lawrence/Champlain	Yes	COW, DOW-CAN, DOW-U.S.	SORE, GAUL, DOW-CAN, DOW-U.S.	SN, GS
8	1000–1800 UTC 6 Mar	Champlain	Yes	COW, DOW-CAN, DOW-U.S.	TROI, SORE, GAUL, DOW-CAN, DOW-U.S.	DZ, RA, FZDZ, FZRA, PL, SG, SN, GS
9	1500 UTC 7 Mar–0200 UTC 8 Mar	St. Lawrence/Champlain	Yes (×2)	COW, DOW-CAN, DOW-U.S.	SORE, GAUL, DOW-CAN, DOW-U.S.	DZ, RA, FZDZ, FZRA, PL, SG, SN
10	0000–0900 UTC 12 Mar	St. Lawrence/Champlain	Yes	DOW-CAN, DOW-U.S.	SORE, GAUL, DOW-CAN, DOW-U.S.	DZ, FZDZ, PL, SG, SN, GS
11	0000–0730 UTC 15 Mar	St. Lawrence/Champlain	No	DOW-CAN, DOW-U.S.	GAUL, JEAN, DOW-U.S.	DZ, RA, SN

<sup>a</sup> FAA-TAIWIN flight.

<sup>b</sup> In collaboration with NASA-IMPACTS.

Valley, and two focusing on the Champlain Valley. The position of the Convair-580 flight tracks and DOW deployments shifted depending on the geographical focus, while most other assets remained fixed (Fig. 1). The synoptic conditions during IOPs included moisture-limited Clipper systems within northwesterly flow, surface cyclones that propagated along stationary frontal boundaries in southwesterly flow, cold-frontal passages, and strong warm-air advection regimes. A wide range of surface p-types, and p-type transitions, were successfully sampled (Table 4). Several weakly forced events primarily consisted of light rain/drizzle and snow (e.g., IOPs 1, 2, 3, 10, 11). A few events included an above-0°C warm layer aloft with sub-0°C air at low levels, facilitating the occurrence of substantial freezing rain and ice pellet accumulations (IOPs, 4, 5, 8, 9). Two events were solely snow events, where observations focused on characterizing mesoscale terrain impacts on precipitation (IOPs 6, 7). Shallow clouds produced drizzle and/or freezing drizzle in some events (e.g., IOP 9).

### Example observations: IOP 5

To illustrate the breadth of observations collected and the types of phenomena sampled during WINTRE-MIX, the following section provides an initial analysis of IOP 5, which took place from 2100 UTC 22 February to 0530 UTC 23 February 2022 (Table 4). We focus on this event as it was well observed by WINTRE-MIX, produced a wide range of p-types in our study domain (including rain/drizzle, freezing rain/drizzle, ice pellets, and ice crystals), and was influenced by mesoscale terrain-modified circulations. The event was also challenging to forecast and had significant societal impacts associated with freezing rain and strong winds, including loss of power to more than 24,000 Hydro Quebec customers (Le Devoir 2023).

**Synoptic overview.** A surface cyclone developed beneath the left-exit region of a 250-hPa jet streak and tracked across southern Quebec on 22–23 February 2022, inducing widespread precipitation across the WINTRE-MIX domain (Fig. 4). As the surface cyclone approached the study domain from the southwest, it led to synoptic-scale forcing for ascent, strong warm-air

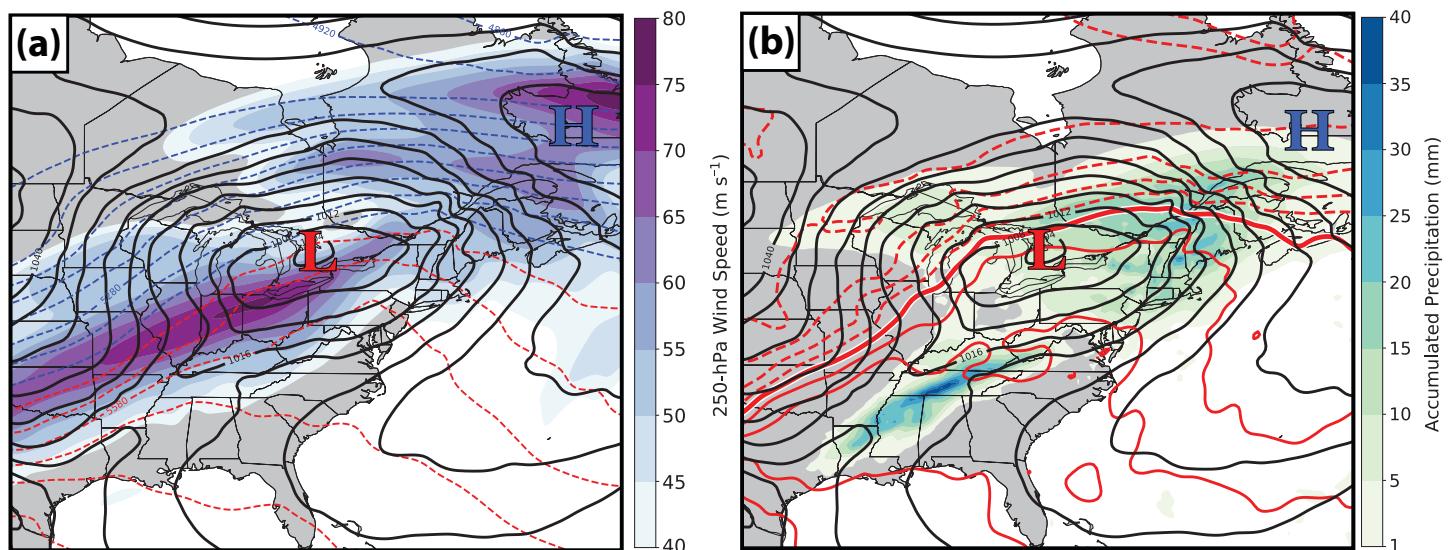
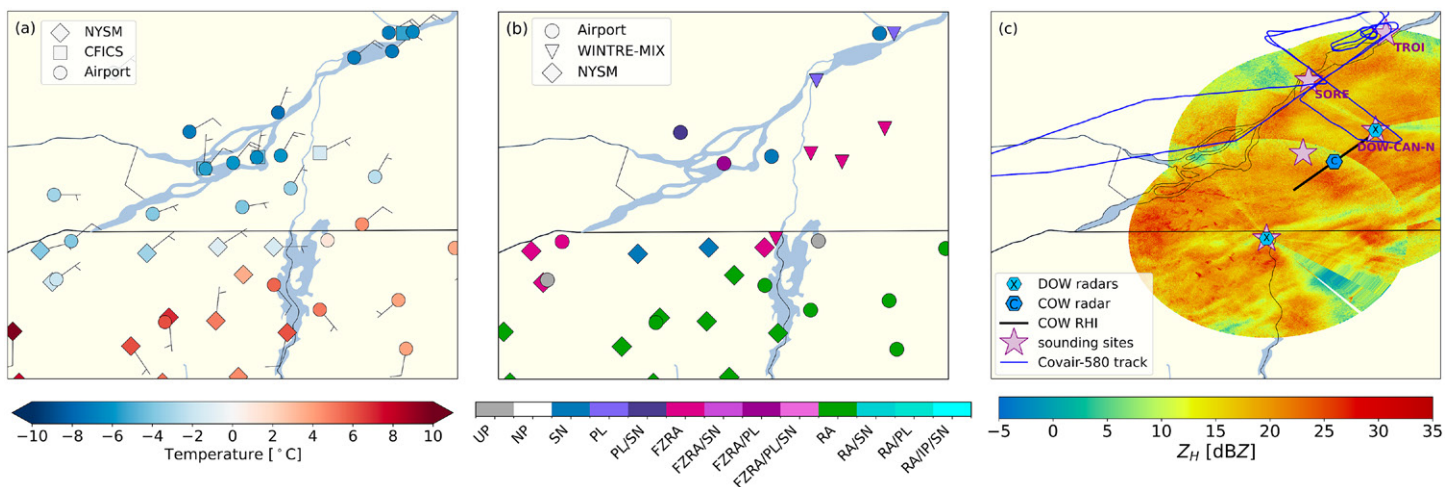


Fig. 4. Overview of synoptic conditions associated with IOP 5. (a) 250-hPa wind speed ( $\text{m s}^{-1}$ ; shaded), mean sea level pressure (every 4 hPa; black contours), and 1,000–500-hPa thickness (every 60 m; dashed blue contours below 5,400 m; dashed red contours above 5,400 m) at 0000 UTC 23 Feb 2022 from the ERA5 dataset. (b) Mean sea level pressure (every 4 hPa; black contours), 850-hPa temperature (every 5°C; dashed red contours where negative, solid red contours where positive) with the 0°C isotherm outlined in white at 0000 UTC 23 Feb 2022. Accumulated precipitation from the ERA5 dataset during IOP 5 (2100 UTC 22 Feb–0600 UTC 23 Feb) is shaded (in mm). Both panels show the locations of surface cyclones (red L) and anticyclones (blue H).

advection, and the development of an elevated above-0°C warm layer (Fig. 4b). Sub-0°C air persisted in the St. Lawrence Valley, however, aided by ageostrophic terrain-channeled northeasterly flow driven by a strong along-valley mean sea level pressure gradient, as has been previously observed during long-duration freezing rain events in the region (e.g., Roebber and Gyakum 2003; Ressler et al. 2012). A local maximum in mean sea level pressure along the valley is indicative of this cold valley air. The vertical alignment of an elevated warm layer atop a shallow sub-0°C layer within the valley facilitated melting of precipitation particles above the surface and the formation of freezing rain and ice pellets within the St. Lawrence Valley during IOP 5. The surface cyclone and upper-level jet streak propagated east of the WINTRE-MIX domain by 0400 UTC 23 February, leading to midlevel subsidence and drying, and the end of widespread precipitation (not shown).

**Mesoscale surface analysis.** Figure 5 provides an overview of mesoscale variations observed at 0000 UTC 23 February 2022, about 3 h after the onset of precipitation in the focus region during IOP 5. Surface stations in the St. Lawrence Valley show sub-0°C temperatures, maintained by northeasterly terrain-channeled flow extending just south of the U.S.–Canada border, while locations to the south show above-0°C temperatures and southerly flow induced by the proximate surface cyclone (Fig. 5a). This mesoscale temperature and wind pattern is similar to that observed during the region’s 1998 freezing rain storm (Roebber and Gyakum 2003). The impacts of these mesoscale temperature variations on p-type can be seen in Fig. 5b, which synthesizes observed and diagnosed p-type from several networks. In the bottom of the St. Lawrence Valley, along the river, where temperatures were coldest, many sites observed ice pellets, as snow melted aloft and the resulting rain became supercooled and refroze in the low-level cold air layer. To the south of the river, including along the U.S.–Canada border, many sites observed freezing rain as the supercooled rain reached the surface before refreezing. Farther south, where near-surface temperatures were above freezing, only rain was observed. Figure 5b also illustrates the challenges of automated p-type diagnosis and the value of manual observations: automated station diagnostics at two NYSM stations and two Canadian airports indicate snow (SN) at this time, whereas nearby manual observations from WINTRE-MIX observers and airport stations with manual observers suggest that these sites were actually experiencing ice pellets (PL) or freezing rain (FZRA).



**Fig. 5. Mesoscale overview of conditions during IOP 5 at 0000 UTC 23 Feb 2022. (a) 2-m temperature and 10-m winds (half barb = 2.5 m s<sup>-1</sup>, full barb = 5 m s<sup>-1</sup>). (b) Observed or estimated p-type. (c) Radar reflectivity factor from 2°-elevation-angle PPI scans, radar and sounding locations, and Convair-580 flight track. In (a) and (b), marker styles indicate the station networks plotted.**

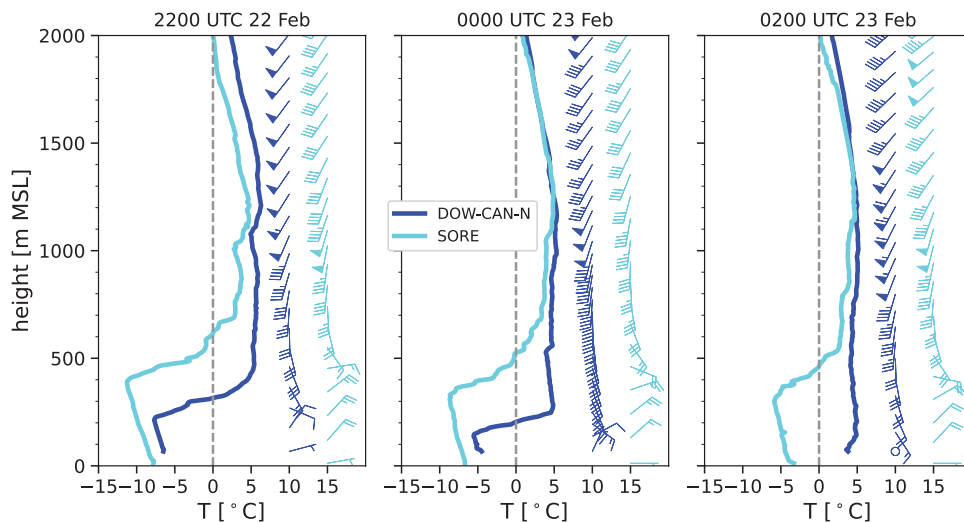


Fig. 6. Example WINTRE-MIX radiosonde profiles of temperature ( $T$ ) and wind (half barb =  $2.5 \text{ m s}^{-1}$ , full barb =  $5 \text{ m s}^{-1}$ ) during IOP 5 at 2200 UTC 22 Feb, 0000 UTC 23 Feb, and 0200 UTC 23 Feb 2022. The sounding locations (SORE, DOW-CAN-N) are indicated in Fig. 5.

The deployment of WINTRE-MIX assets during IOP 5, focused on the St. Lawrence study region, is summarized in Fig. 5c. Sounding and manual observation teams sampled along a transect across the aforementioned mesoscale temperature and p-type transition region. The DOW and COW radar locations allowed for detailed mapping of precipitation and wind structures along and across the St. Lawrence Valley. The Convair-580's flight tracks included along- and across-valley legs at an altitude of about 3.6 km to collect remote sensing measurements and two missed approaches into the Trois-Rivières airport to collect quasi-vertical profiles with in situ sensors.

**Thermodynamic profiles.** The evolution of lower-tropospheric thermodynamic and wind profiles at the Sorel (SORE) and DOW-CAN-N sounding sites is shown in Fig. 6. All soundings show an above- $0^\circ\text{C}$  warm layer from 0.5 to 2.5 km MSL that supported the melting of hydrometeors. This layer exhibited veering south or southwesterly flow, indicative of synoptic-scale warm-air advection. The depth and temperature of this melting layer suggest that hydrometeors were completely melted (Zerr 1997). At 2200 UTC 22 February and 0000 UTC 23 February, both sites show a shallow near-surface sub- $0^\circ\text{C}$  layer with northeasterly terrain-channeled flow. This sub- $0^\circ\text{C}$  layer was only 200–500 m deep, with deeper cold air and lower temperatures in the center of the valley at SORE as compared to at DOW-CAN-N. This surface cold layer facilitated the production of both freezing rain and ice pellets, despite its shallow depth and temperatures being marginal for the latter (Zerr 1997). By 0200 UTC 23 February, the cold layer at DOW-CAN-N rapidly eroded, with a near-surface warming of  $10^\circ\text{C}$  and cessation of northeasterly flow, supporting a transition to rain. The sub- $0^\circ\text{C}$  cold layer was maintained at SORE throughout the IOP, though it warmed and thinned consistent with the persistence of refreezing p-types.

**Surface station perspective.** An example evolution of surface observations at Sorel is shown in Fig. 7. As seen in the soundings, sub- $0^\circ\text{C}$  surface temperatures were maintained at this site throughout the IOP, largely associated with northeasterly terrain-channeled winds (Figs. 7a,b). Manual observers at the site recorded ice pellets (sometimes mixed with freezing drizzle/rain, or ice crystals) from about 2100 UTC 22 February to 0400 UTC 23 February, the period of most significant precipitation (Figs. 7c–i). After this period, a transition

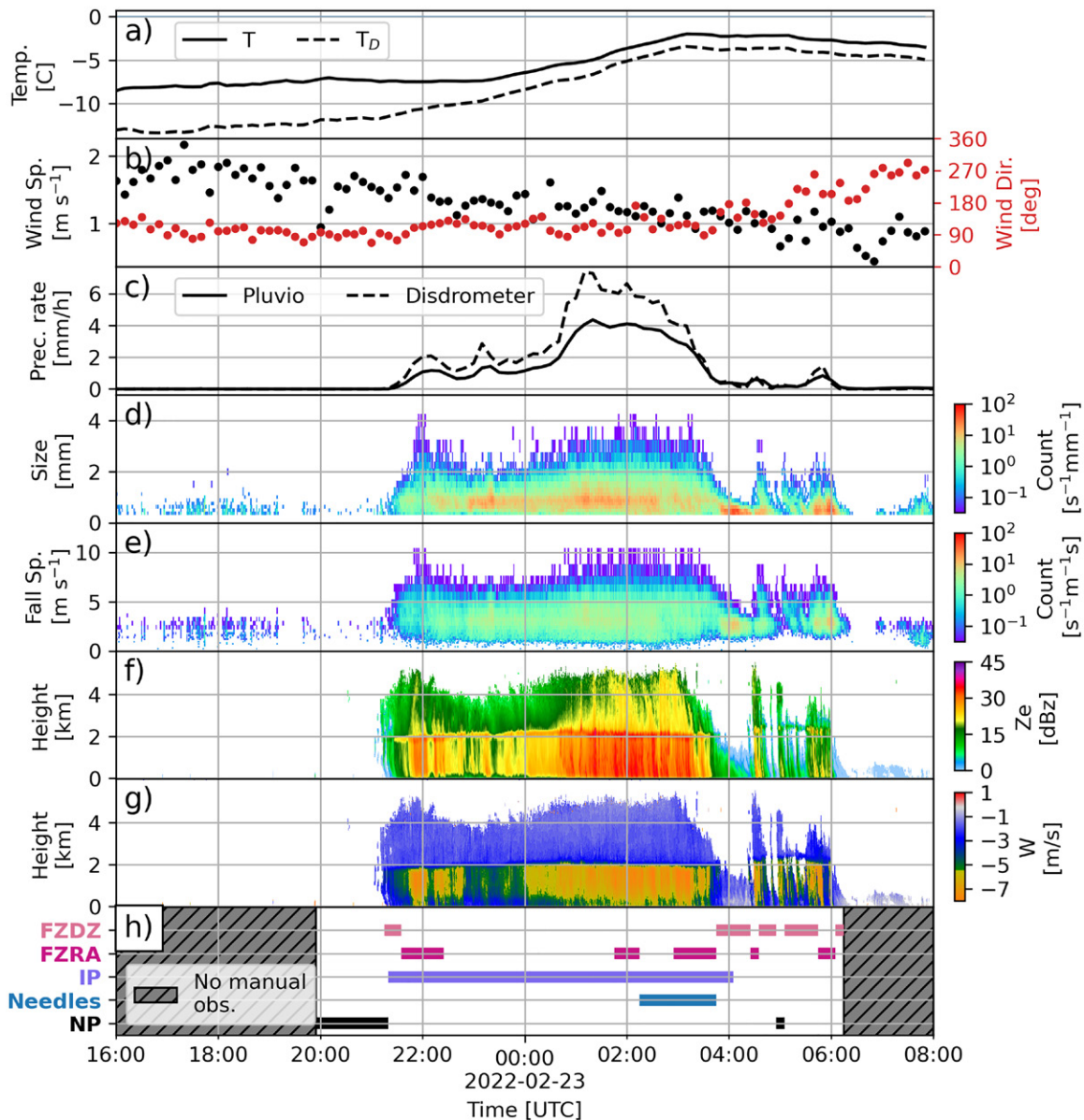


Fig. 7. Evolution of conditions at Sorel (SORE) during IOP 5. (a) Temperature ( $T$ ) and dewpoint temperature ( $T_D$ ), (b) wind speed (black dots) and wind direction (red dots), (c) precipitation rate (in  $\text{mm h}^{-1}$ ) measured by the pluviometer (solid line) and the laser-optical disdrometer (dashed line), (d) normalized size distribution measured by the laser-optical disdrometer, (e) normalized fall speed distribution measured by the laser-optical disdrometer, (f) equivalent reflectivity ( $Z_e$ ) measured by the MRR-Pro, (g) Doppler velocity ( $W$ ) measured by the MRR-Pro, and (h) precipitation types reported by the manual observers.

to lighter precipitation in the form of freezing drizzle and freezing rain was observed. The transitions between p-types are apparent in optical disdrometer observations, with periods of freezing drizzle dominated by small drops with narrow size and fall speed distributions, while periods of freezing rain and ice pellets were associated with broader ranges of hydrometeor sizes and fall speeds (Figs. 7d,e).

Further insight into precipitation processes is provided by MRR-Pro profiling radar observations of reflectivity and Doppler vertical velocity (Figs. 7f,g). During the period of significant precipitation, echo tops extended to 4–5 km MSL, associated with ice aloft, while a clear melting-layer signature (enhanced reflectivity, Doppler velocity gradient) was found near 2 km MSL at the top of the warm nose. Near-surface reductions in reflectivity occurred from about 2200 to 0100 UTC (readily visible from 2200 to 0000 UTC and more

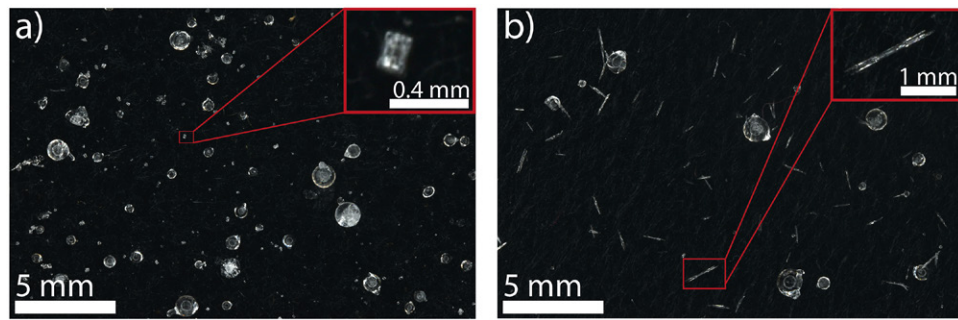


Fig. 8. Two manual hydrometeor macro photographs taken at Sorel site during IOP 5 at (a) 0010 and at (b) 0240 UTC 23 Feb 2022. Both photographs show spherical and quasi-spherical ice pellets. The photograph in (a) is also characterized by the presence of short columnar crystals that were too small to be reported by manual observers while the photograph in (b) is also characterized by needles that were reported by manual observers.

subtly visible from 0000 to 0100 UTC on Fig. 7f). These may be associated with the formation of ice pellets (e.g., Kumjian et al. 2013, 2020; Lachapelle and Thériault 2022). The end of ice pellets and onset of freezing drizzle around 0400 UTC was associated with the onset of synoptic-scale midlevel subsidence (see section “Synoptic overview”) and reductions in humidity above 3.5 km MSL in the 0400 UTC WINTRE-MIX sounding observations (not shown). At Sorel, this was accompanied by a reduction in echo top height, consistent with drying aloft, and the end of a persistent melting-layer signature, suggesting the absence of ice aloft with warmer cloud tops and dominance of liquid phase collision–coalescence in precipitation formation. However, this was occasionally interrupted by brief periods of deeper echoes and freezing rain associated with ice and melting aloft.

Manual hydrometeor macro photographs taken at Sorel documented the morphology of observed ice pellets, including features such as bulges, spicules, and fractures (Fig. 8). Ice crystals were mixed with ice pellets throughout the IOP. The size and habit of these crystals evolved during the event. The first hours of the IOP were characterized by the presence of small columnar crystals  $< 200 \mu\text{m}$  (Fig. 8a) that were too small to be reported by manual observers. Later, needles  $> 1 \text{ mm}$  were reported by the manual observers (Fig. 8b). Needles and other ice crystals have previously been reported together with ice pellets (e.g., Crawford and Stewart 1995; Kumjian et al. 2020; Lachapelle and Thériault 2022). These different ice crystals, potentially generated by secondary ice production through the freezing shattering process (e.g., Lawson et al. 2015; Field et al. 2017) or transported by advection (e.g., Lachapelle and Thériault 2022), might have aided in the formation of ice pellets during IOP 5.

**Radar perspective.** RHI scans from the COW radar provide a vertical cross section of radar reflectivity and radial velocity along the valley (Fig. 9). At 2247 UTC 22 February, the observed reflectivity was stratiform, with modest horizontal variations and a distinct 300–400-m-deep melting layer near 2.3 km AGL and echo tops extending above 8 km AGL (Fig. 9a). At this time, the flow exhibited a strong southwesterly component throughout most of the RHI, with fine-scale layers of vertical shear indicated by changes in radial velocity. A very thin layer of northeasterly flow was observed in the lowest 200 m AGL, consistent with the presence of shallow terrain-channeled cold air observed by the soundings and surface stations. Such shallow layers of reversed valley flow have been observed with radar during wintertime orographic precipitation, where latent cooling from melting and/or evaporation may help to cool the low-level air and facilitate down-valley flow (e.g., Steiner et al. 2003; Thériault et al. 2015; Conrick et al. 2023). However, in this case, latent heat exchange more likely contributes to heating the layer, via hydrometeor refreezing, contributing to its eventual elimination (e.g., McCray et al. 2019; Thériault et al. 2022).

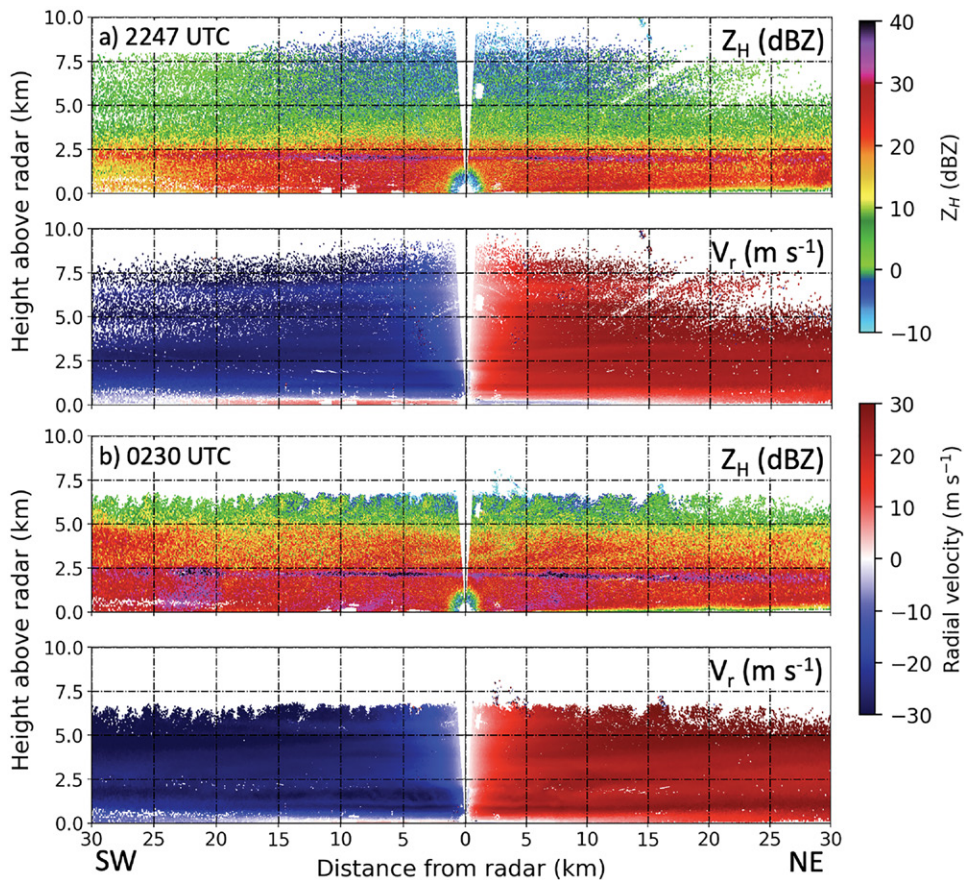


Fig. 9. Along-valley RHIs from COW site showing radar reflectivity ( $Z_H$ ; top panel in each pair) and radial velocity ( $V_r$ ; bottom panel in each pair) at (a) 2247 and (b) 0230 UTC from SW (225°) to NE (45°). Negative (blue) velocity indicate radial velocity toward the radar and positive (red) away from the radar.

The structures seen in the RHIs changed by 0230 UTC when cloud-top generating cells moved into the area and the melting layer became more turbulent (Fig. 9b). Fall streaks, seen as areas of enhanced reflectivity, developed below the generating cells and melting layer. The melting layer slanted downward toward the northeast where it was located at around 2 km AGL compared to the southwest where the melting layer was close to 2.5 km AGL. Winds remained from the southwest throughout the RHIs. As the shallow surface refreezing layer decreased in depth, the associated near surface northeasterly flow signature became absent in the radar RHIs.

**Airborne perspective.** Example airborne observations from one of the Convair-580 missed approaches, from 0049 to 0101 UTC 23 February are shown in Fig. 10. X-band radar observations above and below the aircraft include a clear brightband signature, indicating a 100–200 m thick melting layer at 2 km MSL, with minimal variation in height or depth along the flight track (Fig. 10a). Echo tops extend above 7 km MSL, indicating contributions of ice aloft to precipitation generation. The measured temperature profile includes a deep above-0°C layer from 700 to 2,000 m atop a near-surface sub-0°C layer, with temperatures below  $-8^{\circ}\text{C}$  near the surface, consistent with nearby radiosonde measurements (Fig. 6). Cloud liquid water was observed from just above the top of the warm nose (2.4 km MSL) to the top of the surface-based cold layer.

Optical array probe measurements reveal the vertical evolution of hydrometeors type, shape, and size. At 3,500 m MSL ( $\sim -6^{\circ}\text{C}$ ) and 2,000 m ( $\sim 0^{\circ}\text{C}$ ), hydrometeors appear to be in ice phase with the largest particles composed primarily of aggregates (Fig. 10c). At these altitudes, particle size distributions (PSDs, Fig. 10d) indicate that maximum hydrometeor

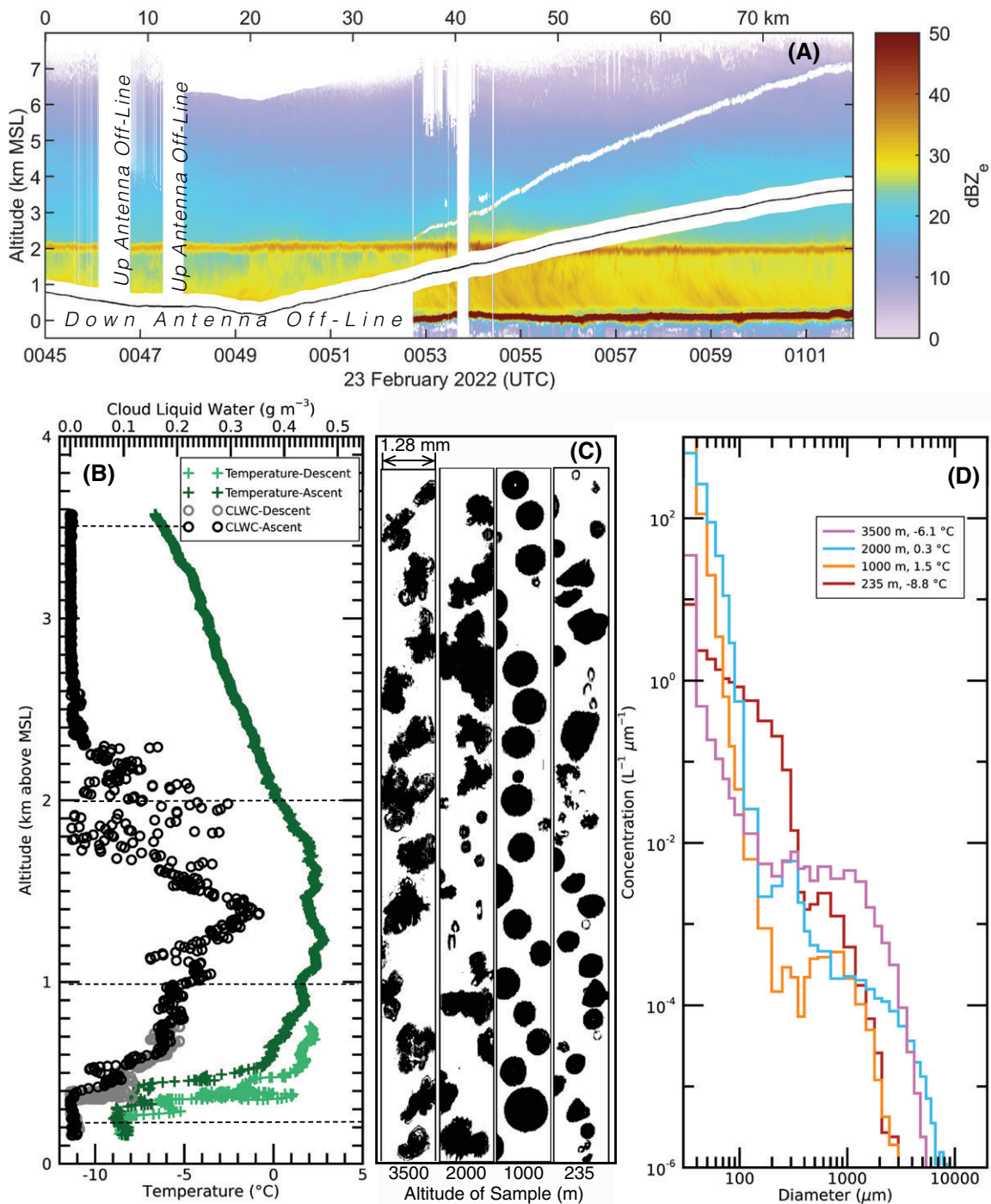


Fig. 10. (a) Vertical cross section of equivalent reflectivity factor measured from the Convair-580 X-band radar during a missed approach from 0049 to 0101 UTC Feb 23. The thin black line indicates the altitude of the aircraft; the white area directly above and below is the ~250-m-wide radar "blind zone." The thick red line near 0 m MSL is return from the surface. (b) Profiles of temperature (green) and cloud liquid water content (black and gray) measured from the Convair-580 during the same period. The horizontal dashed lines in (b) show the altitudes of particle image samples and size distributions shown in (c) and (d). (c) Particle images captured with the 2D-S probe. The scale of the images is shown in the upper-left corner of the panel. Only particles with  $D > 250 \mu\text{m}$  are shown. (d) The particle size distributions based on data from the 2D-S probe for particles up to about 700- $\mu\text{m}$  diameter and from the High Volume Precipitation Spectrometer version 3 (HVPS3) probe for particles larger than 700  $\mu\text{m}$ . The data are averaged over 10-s periods centered on the altitudes indicated in the figure as the aircraft ascended through that altitude.

sizes reach ~8 mm (3.5 km MSL) and ~10 mm (2.0 km MSL). At 1 km MSL, near the middle of the above-0°C layer, spherical shapes suggest that all ice has melted and hydrometeors are entirely liquid, with maximum hydrometeor sizes collapsing to about 3–4 mm, as expected following the melting of large aggregates. In the surface cold layer (235 m MSL, –8.8°C) particle shapes at this altitude are mostly nonspherical, likely associated with the freezing of ice pellets. At this level, the PSD indicates maximum hydrometeor sizes similar to those measured within the warm nose, but also indicates concentrations in the intermediate 100–1,000- $\mu\text{m}$  size range that are substantially larger than in the warm nose. This concentration increase may be due in part to growth by collection in-cloud. Some hydrometeors even appear as half-circles, possibly from shattering of drops upon freezing (e.g., Lawson et al. 2015; Field et al. 2017), which may contribute to the increased number of particles in the 100–1,000- $\mu\text{m}$  size range.

**Open questions and next steps.** The above-described observations of IOP 5 provide an initial peek into the varied processes controlling p-type. They also help to motivate questions that can be addressed with the uniquely rich array of observations collected by WINTRE-MIX during this and other storms. Three example questions and research avenues are listed below.

- *How does p-type predictability depend on synoptic regime?* The large-scale circulation pattern associated with IOP 5 is one of several that can result in freezing rain in the WINTRE-MIX domain. We are examining how the synoptic-scale regime affects the predictability of thermodynamic environments that control p-type. This work is building on WINTRE-MIX case studies with statistical analyses from station data and model ensemble reforecasts.
- *What controls the persistence of the low-level cold air need for refreezing p-types?* A shallow near-surface sub-0°C layer was essential for the occurrence of freezing rain and ice pellets during IOP 5. However, the precise processes that determine the depth, horizontal extent, persistence, and demise of such surface cold layers are not well documented. These processes are being examined in WINTRE-MIX analyses by synthesizing data from our dense network of radiosondes with remote sensing from lidars, radiometers, and Doppler radars to characterize the kinematic and thermodynamic evolution of this cold layer.
- *What microphysical processes determine the initiation of ice pellets after complete melting?* Initial analysis of IOP 5 suggest that ice pellets formed from completely melted hydrometeors in a very shallow sub-0°C layer, with minimum temperatures around –8°C. This requires rapid freezing of rain to form ice pellets at marginal temperatures for ice nucleation. The documentation of ice crystals at the surface and, possibly, shattered ice pellets aloft, suggest a role for secondary ice production. More analysis of data from airborne particle probes, airborne cloud and precipitation radars, surface disdrometers, and ground-based dual-polarization radars should help to illuminate the pathways for ice pellet generation.

To complement observational analyses addressing the above, and other, WINTRE-MIX questions, we are also leveraging mesoscale numerical experiments to generate diagnostic datasets and conduct sensitivity experiments.

### **Broader impacts**

Beyond addressing fundamental science questions, WINTRE-MIX activities are serving to address several broader impacts.

**Model and product evaluation.** Data collected during WINTRE-MIX is being used to improve monitoring, nowcasting, and forecasting of near-0°C precipitation. For instance, field

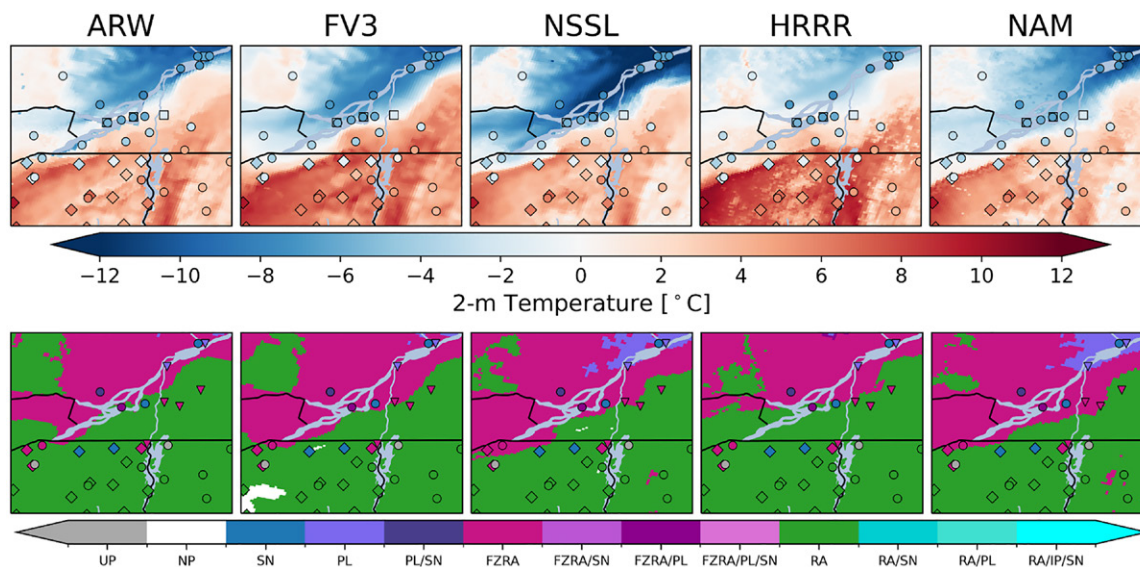


Fig. 11. Evaluation of HREF forecasts of (top) 2-m temperature and (bottom) p-type against surface observations at 0000 UTC 23 Feb 2022. Surface observations and markers are as in Fig. 5. Individual members of the HREF ensemble are indicated by the panel titles. All HREF members show 12-h forecasts, initialized at 1200 UTC 22 Feb 2022.

observations are already being used to provide detailed evaluation of operational mesoscale numerical weather prediction models. Figure 11 compares 12-h forecasts of 2-m temperature and surface p-type from various members of the operational High Resolution Ensemble Forecast (HREF) system to observations during IOP 5. All ensemble members substantially overpredicted temperatures south of the St. Lawrence River near the U.S.–Canada border, leading to widespread rain being forecast in regions where freezing rain was mostly observed. This warm bias appears to be tied to a failure of the members to adequately represent the shallow near-surface cold layer, as comparison with WINTRE-MIX soundings indicate much smaller temperature errors in the warm nose and aloft (not shown). Large member-to-member differences are found in the magnitude of the near-surface warm bias and in temperatures along the St. Lawrence Valley. Furthermore, only two members (NSSL and NAM) successfully predicted the occurrence of ice pellets manually observed at the SORE and TROI sites by WINTRE-MIX researchers. Continuing to leverage WINTRE-MIX observations to understand the sources of model biases can help to inform model development (e.g., via improvements to parameterized physics and/or data assimilation).

Even with the relatively dense surface network in the region, mapping out the precise locations of p-type transitions can be challenging, especially for ice pellets, which are not readily diagnosed by most stations (e.g., NOAA 1998). Other ongoing and planned applied research efforts include evaluating and improving observational p-type and icing diagnostics (with the New York State Mesonet), radar retrievals (with Environment and Climate Change Canada), and aircraft icing diagnostics (with FAA’s TAIWIN Demo project). Improvements to observational diagnostics may feed back onto forecast model development, as they improve the datasets used to evaluate these models.

**Bridging gaps in research to operations.** A critical partner in bridging the gap between WINTRE-MIX research and operations is the National Weather Service (NWS), due to their clear interest in accurately forecasting precipitation type and amount. In addition to sharing our results on HREF model biases with NWS forecasters, WINTRE-MIX has begun to create products and tools that directly assist NWS in their mission, such as real-time icing maps created with NYSM observations using the method of Sanders and Barjenbruch (2016).

To facilitate further connections between the research and operational communities, a stakeholder workshop was held at UAlbany in May 2023 with presentations and participation from a variety of sectors including the local NWS forecast office, transportation (New York State Department of Transportation), energy (an area electric utility), private sector meteorology (including forensics and disaster management), related field campaigns (IMPACTS and TAIWIN), NYSM, and various academics, including several using artificial intelligence approaches to diagnose and forecast winter p-type and road conditions. All presenters were asked to provide a “wish list” to the research community on the topic of winter precipitation forecasting. Three common themes among these lists were more observations and diagnostics of precipitation type, improved metrics for expressing forecast confidence/uncertainty, and better understanding of how climate change may alter near-0°C precipitation. As a step toward addressing the first theme, WINTRE-MIX partnered with the NYSM to re-deploy freezing rain sensors at NYSM stations to aid in monitoring and in the evaluation of diagnostic p-type and ice accretion products. The second theme is being addressed through WINTRE-MIX analysis of synoptic-scale predictability and mesoscale numerical model performance.

**Education and outreach.** WINTRE-MIX is contributing to scientific training, literacy, and engagement through education of undergraduate and graduate students, postdoc mentoring, educational outreach events, and citizen science observations. Thirty students from the United States and Canada, including six undergraduate students, participated in WINTRE-MIX, with many gaining their first field project experience. They were involved in instrument deployment, data collection during the IOPs, weather briefing preparation and presentation, and data quality control and analysis efforts following the campaign. WINTRE-MIX also engaged citizen scientists in data collection. In particular, WINTRE-MIX coordinated with the Canadian Community Collaborative Rain, Hail, and Snow Network (CoCoRaHS) and the National Weather Service’s Burlington, Vermont, forecast office to advertise the campaign and explain our need for citizen observations, including through CoCoRaHS and the mPING application (Elmore et al. 2014).

WINTRE-MIX conducted two educational outreach events. An open house event was hosted on the University at Albany campus, attended by local media and members of the campus community, and included a visit by one of the DOW radars and a demonstration radiosonde launch (Fig. 12). Another event, hosted at the NRC Flight Research Laboratory in Ottawa, allowed students and researchers from the participating academic institutions to tour the NRC-Convair-580 and learn about airborne sensors and atmospheric observations (Fig. 12). These activities were also shared with the general public via traditional media coverage (newspaper, television, radio; Fig. 12) and social media ([https://twitter.com/WINTRE\\_MIX](https://twitter.com/WINTRE_MIX)).

Educational activities associated with WINTRE-MIX are ongoing. Undergraduate students are using the data in research projects (e.g., Barletta 2023). Data from the field project are being incorporated into lectures and activities to help teach topics in mesoscale and synoptic meteorology, radar, cloud physics, and forecasting.

### **Concluding remarks**

Through a multi-institutional and international effort, WINTRE-MIX successfully collected unique and detailed data at the surface and aloft for 11 near-0°C precipitation events spanning a wide range of precipitation types and transitions. Ongoing research will leverage this data to improve our fundamental understanding of the processes determining precipitation type during “wintry mix” conditions. Applied research will work to improve tools for observing, forecasting, and mitigating the impacts associated with winter precipitation.



Fig. 12. Photos from WINTRE-MIX education and outreach events: (top left) Radio interview with Radio-Canada at Sorel, (top right) open house event with DOW radar at University at Albany, and (bottom) students and researchers with Convair-580 at NRC Flight Research Laboratory.

Datasets collected for WINTRE-MIX are available (as of 17 March 2023) through a publicly accessible archive [https://data.eol.ucar.edu/master\\_lists/generated/wintre-mix/](https://data.eol.ucar.edu/master_lists/generated/wintre-mix/). Collaborations with others interested in using WINTRE-MIX data for basic and applied research are welcome.

**Acknowledgments.** We thank M. Kumjian and two anonymous reviewers for their constructive feedback that helped to improve the manuscript. WINTRE-MIX research was supported by NSF (AGS Grants 2114011, 2113995, and 2114006), Canada Research Chairs Program, NSERC, FRQNT, and the NRC Aeronautical Product Development and Certification (APDC) program. NCAR's Earth Observing Laboratory, sponsored by the National Science Foundation, provided operational, technical, and scientific support including the Field Catalog, the Field Data Archive and related staffing support. CFICS stations are funded by the Canada Foundation of Innovation (CFI) Adaptable Earth Observation System. NYSM stations are supported by the NYS Division of Homeland Security and Emergency Services, the State of New York, and the University at Albany. C. McCray provided the data used to generate Fig. 2. North-view Weather and the NWS-BTV forecast office provided products that aided WINTRE-MIX forecasting. Alexandre Touchette, Radio-Canada, provided permission for use of the top-left photo in Fig. 12. Site hosts that facilitated deployment of WINTRE-MIX instrumentation on their properties include J.J. Lemyre and L. Roberge (SORE), the Miner Institute (CHAZ), S. Gauthier (DOW-CAN), the McGill University Gault Nature Reserve (GAUL). The projects NASA-IMPACTS (including L. McMurdie and J. Finlon) and FAA-TAIWIN Demo (including S. DiVito, B. Bernstein, S. Landolt) provided various forms of helpful coordination and collaboration. The ECCC instrumentation at Sorel was led by R. Reed, with help from C. Lachapelle and J. Girouard. McGill CFICS staff (C. Giurgiu and E. Bigras) and UAlbany NYSM staff (N. Bain, S. McKim, K. Hemker) provided assistance with mesonet data and instrumentation. Researchers, pilots, engineering, management, operation staff and students from NRC contributed to successful

Convair-580 operations, including K. Ranjbar, K. Bala, N. Bliankinshtein, A. Brown, R. Sherwood, B. Carrothers, E. Roux, D. MacDonald, S. Ingram, T. Van Westerop, D. Hoyi, L. Fleury, and K. Bavanathan. Contributions to FARM radar data management and operations were made by J. Aikins, P. Robinson, C. Smith, R. Aikins, T. White, B. Pereira, and V. Meunier. Finally, we thank the large team of students and postdocs that contributed to field operations, including B. Han, M. Brewer, B. Filipiak, R. Eldridge, E. Potter, Y. Rojas, M. Barletta, J. England, S. Liotta, M. Schiede, S. Boschulte, R. Baiman, A. Fagerson, C. Reiher, T. Whittock III, B. Dettmann, C. Hohman, M. Girouard, S. Basnet, E. Cardinal, K. Veilleux, H. Thompson, C. Coulbury, H. Carr, D. Fraser, J. Liu, Y. Low, K. Simzer, B. Ward, J. Wray, and C. Z. Jing. The WINTRE-MIX logo was designed by D. Durler.

**Data availability statement.** All WINTRE-MIX observations presented are available from the WINTRE-MIX data archive ([https://data.eol.ucar.edu/master\\_lists/generated/wintre-mix/](https://data.eol.ucar.edu/master_lists/generated/wintre-mix/)). Reports and quicklook plots of WINTRE-MIX data are available from the WINTRE-MIX field catalog (<http://catalog.eol.ucar.edu/wintre-mix>). NYSM data are available, with some restrictions, from <http://nysmesonet.org/weather/requestdata>. mPING data are available from <https://mping.ou.edu/static/mping/access.html>. Other data presented are available from the following sources: archived HREF forecasts (<https://data.nssl.noaa.gov/thredds/catalog/FRDD.html>), airport observations (<https://mesonet.agron.iastate.edu/request/download.phtml>), and ERA-5 (Hersbach et al. 2018a,b).

## References

- Baibakov, K., M. Wolde, C. Nguyen, A. Korolev, Z. Wang, and P. Wechsler, 2016: Performance of a compact elastic 355 nm airborne lidar in tropical and mid-latitude clouds. *Proc. SPIE*, **10006**, 100060C, <https://doi.org/10.1117/12.2242112>.
- Barletta, M., 2023: Investigating the difference between members in the High-Resolution Rapid Refresh Ensemble (HRRRE) during the February 23rd, 2022 winter storm. M.S. thesis, Dept. of Atmospheric and Environmental Sciences, University at Albany, 40 pp., [https://scholarsarchive.library.albany.edu/honorscollege\\_daes/26](https://scholarsarchive.library.albany.edu/honorscollege_daes/26).
- Bernstein, B., and Coauthors, 2021: The In-Cloud Icing and Large-Drop Experiment science and operations plan. Federal Aviation Administration Tech. Rep. DOT/FAA/TC-21/29, U.S. Department of Transportation, 174 pp., <https://www.tc.faa.gov/its/worldpac/techrpt/tc21-29.pdf>.
- Bernstein, B. C., 2000: Regional and local influences on freezing drizzle, freezing rain, and ice pellet events. *Wea. Forecasting*, **15**, 485–508, [https://doi.org/10.1175/1520-0434\(2000\)015<0485:RALIOF>2.0.CO;2](https://doi.org/10.1175/1520-0434(2000)015<0485:RALIOF>2.0.CO;2).
- Brotzge, J. A., and Coauthors, 2020: A technical overview of the New York State Mesonet standard network. *J. Atmos. Oceanic Technol.*, **37**, 1827–1845, <https://doi.org/10.1175/JTECH-D-19-0220.1>.
- Cai, Y., D. C. Montague, W. Mooiweer-Bryan, and T. Deshler, 2008: Performance characteristics of the ultra high sensitivity aerosol spectrometer for particles between 55 and 800 nm: Laboratory and field studies. *J. Aerosol Sci.*, **39**, 759–769, <https://doi.org/10.1016/j.jaerosci.2008.04.007>.
- Changnon, S. A., 2003: Characteristics of ice storms in the United States. *J. Appl. Meteor.*, **42**, 630–639, [https://doi.org/10.1175/1520-0450\(2003\)042<0630:COISIT>2.0.CO;2](https://doi.org/10.1175/1520-0450(2003)042<0630:COISIT>2.0.CO;2).
- Cholette, M., H. Morrison, J. A. Milbrandt, and J. M. Thériault, 2019: Parameterization of the bulk liquid fraction on mixed-phase particles in the Predicted Particle Properties (P3) scheme: Description and idealized simulations. *J. Atmos. Sci.*, **76**, 561–582, <https://doi.org/10.1175/JAS-D-18-0278.1>.
- Cober, S. G., J. W. Strapp, and G. A. Isaac, 1996: An example of supercooled drizzle drops formed through a collision-coalescence process. *J. Appl. Meteor.*, **35**, 2250–2260, [https://doi.org/10.1175/1520-0450\(1996\)035<2250:AEOSDD>2.0.CO;2](https://doi.org/10.1175/1520-0450(1996)035<2250:AEOSDD>2.0.CO;2).
- Conrick, R., J. P. Boomgard-Zagrodnik, and L. A. McMurdie, 2023: Observed and simulated characteristics of down-valley flow within stratiform precipitation over the Olympic Peninsula. *Mon. Wea. Rev.*, **151**, 1407–1426, <https://doi.org/10.1175/MWR-D-22-0229.1>.
- Cortinas, J. V., Jr., B. C. Bernstein, C. C. Robbins, and J. W. Strapp, 2004: An analysis of freezing rain, freezing drizzle, and ice pellets across the United States and Canada: 1976–90. *Wea. Forecasting*, **19**, 377–390, [https://doi.org/10.1175/1520-0434\(2004\)019<0377:AAOFRF>2.0.CO;2](https://doi.org/10.1175/1520-0434(2004)019<0377:AAOFRF>2.0.CO;2).
- Crawford, R. W., and R. E. Stewart, 1995: Precipitation type characteristics at the surface in winter storms. *Cold Reg. Sci. Technol.*, **23**, 215–229, [https://doi.org/10.1016/0165-232X\(94\)00014-0](https://doi.org/10.1016/0165-232X(94)00014-0).
- Damiani, R., and S. Haimov, 2006: A high-resolution dual-Doppler technique for fixed multi-antenna airborne radar. *IEEE Trans. Geosci. Remote Sens.*, **44**, 3475–3489, <https://doi.org/10.1109/TGRS.2006.881745>.
- DeGaetano, A. T., 2000: Climatic perspective and impacts of the 1998 Northern New York and New England ice storm. *Bull. Amer. Meteor. Soc.*, **81**, 237–254, [https://doi.org/10.1175/1520-0477\(2000\)081<0237:CPAIOT>2.3.CO;2](https://doi.org/10.1175/1520-0477(2000)081<0237:CPAIOT>2.3.CO;2).
- Durrán, D. R., P. A. Reinecke, and J. D. Doyle, 2013: Large-scale errors and mesoscale predictability in Pacific Northwest snowstorms. *J. Atmos. Sci.*, **70**, 1470–1487, <https://doi.org/10.1175/JAS-D-12-0202.1>.
- Elmore, K. L., Z. L. Flamig, V. Lakshmanan, B. T. Kaney, V. Farmer, H. D. Reeves, and L. P. Rothfus, 2014: MPING: Crowd-sourcing weather reports for research. *Bull. Amer. Meteor. Soc.*, **95**, 1335–1342, <https://doi.org/10.1175/BAMS-D-13-00014.1>.
- FAA, 2015: Pilot guide: Flight in icing conditions. Federal Aviation Administration Advisory Circular 91-74B, U.S. Department of Transportation, 63 pp., [https://www.faa.gov/documentLibrary/media/Advisory\\_Circular/AC\\_91-74B.pdf](https://www.faa.gov/documentLibrary/media/Advisory_Circular/AC_91-74B.pdf).
- Field, P. R., and Coauthors, 2017: Secondary ice production: Current state of the science and recommendations for the future. *Ice Formation and Evolution in Clouds and Precipitation: Measurement and Modeling Challenges*, Meteor. Monogr., No. 58, Amer. Meteor. Soc., <https://doi.org/10.1175/AMSMONOGRAPHS-D-16-0014.1>.
- Gibson, S. R., and R. E. Stewart, 2007: Observations of ice pellets during a winter storm. *Atmos. Res.*, **85**, 64–76, <https://doi.org/10.1016/j.atmosres.2006.11.004>.
- Gultepe, I., M. Agelin-Chaab, J. Komar, G. Elfstrom, F. Boudala, and B. Zhou, 2019: A meteorological supersite for aviation and cold weather applications. *Pure Appl. Geophys.*, **176**, 1977–2015, <https://doi.org/10.1007/s00024-018-1880-3>.
- Gyakum, J. R., and P. J. Roebber, 2001: The 1998 Ice Storm—Analysis of a planetary-scale event. *Mon. Wea. Rev.*, **129**, 2983–2997, [https://doi.org/10.1175/1520-0493\(2001\)129<2983:TISAOA>2.0.CO;2](https://doi.org/10.1175/1520-0493(2001)129<2983:TISAOA>2.0.CO;2).
- Henson, W., R. Stewart, B. Kochtubajda, and J. Thériault, 2011: The 1998 Ice Storm: Local flow fields and linkages to precipitation. *Atmos. Res.*, **101**, 852–862, <https://doi.org/10.1016/j.atmosres.2011.05.014>.
- Hersbach, H., and Coauthors, 2018a: ERA5 hourly data on pressure levels from 1959 to present. Copernicus Climate Change Service (C3S) Climate Data Store (CDS), accessed 30 May 2023, <https://doi.org/10.24381/cds.bd0915c6>.
- , and Coauthors, 2018b: ERA5 hourly data on single levels from 1959 to present. Copernicus Climate Change Service (C3S) Climate Data Store (CDS), accessed 30 May 2023, <https://doi.org/10.24381/cds.adbb2d47>.
- Ikeda, K., M. Steiner, J. Pinto, and C. Alexander, 2013: Evaluation of cold-season precipitation forecasts generated by the hourly updating High-Resolution Rapid Refresh Model. *Wea. Forecasting*, **28**, 921–939, <https://doi.org/10.1175/WAF-D-12-00085.1>.
- Korolev, A., J. W. Strapp, G. A. Isaac, and E. Emery, 2013: Improved airborne hot-wire measurements of ice water content in clouds. *J. Atmos. Oceanic Technol.*, **30**, 2121–2131, <https://doi.org/10.1175/JTECH-D-13-00007.1>.
- Kumjian, M. R., A. V. Ryzhkov, H. D. Reeves, and T. J. Schuur, 2013: A dual-polarization radar signature of hydrometeor refreezing in winter storms. *J. Appl. Meteor. Climatol.*, **52**, 2549–2566, <https://doi.org/10.1175/JAMC-D-12-0311.1>.
- , D. M. Tobin, M. Oue, and P. Kollias, 2020: Microphysical insights into ice pellet formation revealed by fully polarimetric Ka-band Doppler radar. *J. Appl. Meteor. Climatol.*, **59**, 1557–1580, <https://doi.org/10.1175/JAMC-D-20-0054.1>.
- Lachapelle, M., and J. M. Thériault, 2022: Characteristics of precipitation particles and microphysical processes during the 11–12 January 2020 Ice Pellet Storm in the Montréal Area, Québec, Canada. *Mon. Wea. Rev.*, **150**, 1043–1059, <https://doi.org/10.1175/MWR-D-21-0185.1>.
- Landolt, S. D., J. S. Lave, D. Jacobson, A. Gaydos, S. DiVito, and D. Porter, 2019: The impacts of automation on present weather-type observing capabilities across the conterminous United States. *J. Appl. Meteor. Climatol.*, **58**, 2699–2715, <https://doi.org/10.1175/JAMC-D-19-0170.1>.
- Lawson, R. P., S. Woods, and H. Morrison, 2015: The microphysics of ice and precipitation development in tropical cumulus clouds. *J. Atmos. Sci.*, **72**, 2429–2445, <https://doi.org/10.1175/JAS-D-14-0274.1>.
- Le Devoir, 2023: Des abonnés d’hydro-québec sont rebranchés après des pannes causées par le verglas. *Le Devoir*, 23 February, <https://www.ledevoir.com/environnement/678366/la-pluie-verglacante-entraîne-des-pannes-de-courant-au-quebec>.
- Lott, N., D. Ross, and A. Graumann, 1998: Eastern U.S. flooding and ice storm January 1998. NOAA National Climatic Data Center Special Rep., 6 pp., <https://www.ncei.noaa.gov/pub/data/extremeevents/specialreports/Eastern-US-Flooding-and-Ice-Storm-January1998.pdf>.
- McCray, C. D., E. H. Atallah, and J. R. Gyakum, 2019: Long-duration freezing rain events over North America: Regional climatology and thermodynamic evolution. *Wea. Forecasting*, **34**, 665–681, <https://doi.org/10.1175/WAF-D-18-0154.1>.

- , J. R. Gyakum, and E. H. Atallah, 2020: Regional thermodynamic characteristics distinguishing long- and short-duration freezing rain events over North America. *Wea. Forecasting*, **35**, 657–671, <https://doi.org/10.1175/WAF-D-19-0179.1>.
- McMurdie, L. A., and Coauthors, 2022: Chasing snowstorms: The Investigation of Microphysics and Precipitation for Atlantic Coast-Threatening Snowstorms (IMPACTS) campaign. *Bull. Amer. Meteor. Soc.*, **103**, E1243–E1269, <https://doi.org/10.1175/BAMS-D-20-0246.1>.
- Mekis, E., R. E. Stewart, J. M. Theriault, B. Kochtubajda, B. R. Bonsal, and Z. Liu, 2020: Near-0°C surface temperature and precipitation type patterns across Canada. *Hydrol. Earth Syst. Sci.*, **24**, 1741–1761, <https://doi.org/10.5194/hess-24-1741-2020>.
- Milbrandt, J. A., J. Theriault, and R. Mo, 2014: Modeling the phase transition associated with melting snow in a 1D kinematic framework: Sensitivity to the microphysics. *Pure Appl. Geophys.*, **171**, 303–322, <https://doi.org/10.1007/s00024-012-0552-y>.
- Minder, J. R., and D. E. Kingsmill, 2013: Mesoscale variations of the atmospheric snow-line over the northern Sierra Nevada: Multi-year statistics, case study, and mechanisms. *J. Atmos. Sci.*, **70**, 916–938, <https://doi.org/10.1175/JAS-D-12-0194.1>.
- Mitra, S. K., O. Vohl, M. Ahr, and H. R. Pruppacher, 1990: A wind-tunnel and theoretical-study of the melting behavior of atmospheric ice particles. Part 4: Experiment and theory for snow flakes. *J. Atmos. Sci.*, **47**, 584–591, [https://doi.org/10.1175/1520-0469\(1990\)047<0584:AWTATS>2.0.CO;2](https://doi.org/10.1175/1520-0469(1990)047<0584:AWTATS>2.0.CO;2).
- Nguyen, C. M., M. Wolde, A. Battaglia, L. Nichman, N. Bliankinshtein, S. Haimov, K. Bala, and D. Schuettmeyer, 2022: Coincident in situ and triple-frequency radar airborne observations in the Arctic. *Atmos. Meas. Tech.*, **15**, 775–795, <https://doi.org/10.5194/amt-15-775-2022>.
- Nichman, L., and Coauthors, 2023: Airborne platform for ice-accretion and coatings tests with ultrasonic readings (PICTUR). SAE Tech. Paper, SAE International, 12 pp., <https://www.sae.org/publications/technical-papers/content/2023-01-1431/>.
- NOAA, 1998: Automated Surface Observing System (ASOS) user's guide. National Oceanic and Atmospheric Administration, 61 pp., <https://www.weather.gov/media/asos/aum-toc.pdf>.
- Ralph, F. M., and Coauthors, 2005: Improving short-term (0–48 h) cool-season quantitative precipitation forecasting – Recommendations from a USWRP workshop. *Bull. Amer. Meteor. Soc.*, **86**, 1619–1632, <https://doi.org/10.1175/BAMS-86-11-1615>.
- Rasmussen, R., and Coauthors, 2012: How well are we measuring snow? The NOAA/FAA/NCAR winter precipitation test bed. *Bull. Amer. Meteor. Soc.*, **93**, 811–829, <https://doi.org/10.1175/BAMS-D-11-00052.1>.
- Rasmussen, R. M., I. Geresdi, G. Thompson, K. Manning, and E. Karplus, 2002: Freezing drizzle formation in stably stratified layer clouds: The role of radiative cooling of cloud droplets, cloud condensation nuclei, and ice initiation. *J. Atmos. Sci.*, **59**, 837–860, [https://doi.org/10.1175/1520-0469\(2002\)059<0837:FDFISS>2.0.CO;2](https://doi.org/10.1175/1520-0469(2002)059<0837:FDFISS>2.0.CO;2).
- Rauber, R. M., L. S. Olthoff, M. K. Ramamurthy, D. Miller, and K. E. Kunkel, 2001: A synoptic weather pattern and sounding-based climatology of freezing precipitation in the United States East of the Rocky Mountains. *J. Appl. Meteor.*, **40**, 1724–1747, [https://doi.org/10.1175/1520-0450\(2001\)040<1724:ASWPAS>2.0.CO;2](https://doi.org/10.1175/1520-0450(2001)040<1724:ASWPAS>2.0.CO;2).
- Reeves, H. D., K. L. Elmore, A. Ryzhkov, T. Schuur, and J. Krause, 2014: Sources of uncertainty in precipitation-type forecasting. *Wea. Forecasting*, **29**, 936–953, <https://doi.org/10.1175/WAF-D-14-00007.1>.
- , A. V. Ryzhkov, and J. Krause, 2016: Discrimination between winter precipitation types based on spectral-bin microphysical modeling. *J. Appl. Meteor. Climatol.*, **55**, 1747–1761, <https://doi.org/10.1175/JAMC-D-16-0044.1>.
- Ressler, G. M., S. M. Milrad, E. H. Atallah, and J. R. Gyakum, 2012: Synoptic-scale analysis of freezing rain events in Montreal, Quebec, Canada. *Wea. Forecasting*, **27**, 362–378, <https://doi.org/10.1175/WAF-D-11-00071.1>.
- Roebber, P. J., and J. R. Gyakum, 2003: Orographic influences on the mesoscale structure of the 1998 ice storm. *Mon. Wea. Rev.*, **131**, 27–50, [https://doi.org/10.1175/1520-0493\(2003\)131<0027:OIOTMS>2.0.CO;2](https://doi.org/10.1175/1520-0493(2003)131<0027:OIOTMS>2.0.CO;2).
- Sanders, K. J., and B. L. Barjenbruch, 2016: Analysis of ice-to-liquid ratios during freezing rain and the development of an ice accumulation model. *Wea. Forecasting*, **31**, 1041–1060, <https://doi.org/10.1175/WAF-D-15-0118.1>.
- Shin, K., K. Kim, J. J. Song, and G. Lee, 2022: Classification of precipitation types based on machine learning using dual-polarization radar measurements and thermodynamic fields. *Remote Sens.*, **14**, 3820, <https://doi.org/10.3390/rs14153820>.
- Shingler, T., and Coauthors, 2012: Characterisation and airborne deployment of a new counterflow virtual impactor inlet. *Atmos. Meas. Tech.*, **5**, 1259–1269, <https://doi.org/10.5194/amt-5-1259-2012>.
- Steiner, M., O. Bousquet, R. A. Houze Jr., B. F. Smull, and M. Mancin, 2003: Airflow within major alpine river valleys under heavy rainfall. *Quart. J. Roy. Meteor. Soc.*, **129**, 411–431, <https://doi.org/10.1256/qj.02.08>.
- Stewart, R. E., J. M. Theriault, and W. Henson, 2015: On the characteristics of and processes producing winter precipitation types near 0°C. *Bull. Amer. Meteor. Soc.*, **96**, 623–639, <https://doi.org/10.1175/BAMS-D-14-00032.1>.
- Theriault, J. M., R. E. Stewart, and W. Henson, 2010: On the dependence of winter precipitation types on temperature, precipitation rate, and associated features. *J. Appl. Meteor. Climatol.*, **49**, 1429–1442, <https://doi.org/10.1175/2010JAMC2321.1>.
- , J. A. Milbrandt, J. Doyle, J. R. Minder, G. Thompson, N. Sarkadi, and I. Geresdi, 2015: Impact of melting snow on the valley flow field and precipitation phase transition. *Atmos. Res.*, **156**, 111–124, <https://doi.org/10.1016/j.atmosres.2014.12.006>.
- , V. McFadden, H. D. Thompson, and M. Cholette, 2022: Meteorological factors responsible for major power outages during a severe freezing rain storm over eastern Canada. *J. Appl. Meteor. Climatol.*, **61**, 1239–1255, <https://doi.org/10.1175/JAMC-D-21-0217.1>.
- Tobin, D. M., M. R. Kumjian, and A. W. Black, 2021: Effects of precipitation type on crash relative risk estimates in Kansas. *Accid. Anal. Prev.*, **151**, 105946, <https://doi.org/10.1016/j.aap.2020.105946>.
- Tootill, D., and D. J. Kirshbaum, 2022: Ensemble sensitivity of precipitation type to initial conditions for a major freezing rain event in Montreal. *Mon. Wea. Rev.*, **150**, 1761–1780, <https://doi.org/10.1175/MWR-D-21-0254.1>.
- Wang, J., J. Brotzge, J. Shultis, and N. Bain, 2021: Enhancing icing detection and characterization using the New York State Mesonet. *J. Atmos. Oceanic Technol.*, **38**, 1499–1514, <https://doi.org/10.1175/JTECH-D-20-0215.1>.
- Wolde, M., and A. Pazmany, 2005: NRC dual-frequency airborne radar for atmospheric research. *32nd Conf. on Radar Meteorology*, Albuquerque, NM, Amer. Meteor. Soc., P1R.9, <https://ams.confex.com/ams/32Rad11Meso/webprogram/Paper96918.html>.
- , A. Battaglia, C. Nguyen, A. L. Pazmany, and A. Illingworth, 2019: Implementation of polarization diversity pulse-pair technique using airborne W-band radar. *Atmos. Meas. Tech.*, **12**, 253–269, <https://doi.org/10.5194/amt-12-253-2019>.
- Wurman, J., and Coauthors, 2021: The Flexible Array of Radars and Mesonets (FARM). *Bull. Amer. Meteor. Soc.*, **102**, E1499–E1525, <https://doi.org/10.1175/BAMS-D-20-0285.1>.
- Zerr, R. J., 1997: Freezing rain: An observational and theoretical study. *J. Appl. Meteor.*, **36**, 1647–1661, [https://doi.org/10.1175/1520-0450\(1997\)036<1647:FRAOAT>2.0.CO;2](https://doi.org/10.1175/1520-0450(1997)036<1647:FRAOAT>2.0.CO;2).